Materials Today Energy 19 (2021) 100583

Contents lists available at ScienceDirect

Materials Today Energy

journal homepage: www.journals.elsevier.com/materials-today-energy/

Photovoltaic technologies for flexible solar cells: beyond silicon

Sangmo Kim, Hoang Van Quy, Chung Wung Bark*

Department of Electrical Engineering, Gachon University, Seongnam, 13120, Republic of Korea

ARTICLE INFO

Article history:
Received 15 July 2020
Received in revised form
29 October 2020
Accepted 8 November 2020
Available online 13 November 2020

Keywords:
Flexible
PV system
Module
Fabrication
Beyond silicon

ABSTRACT

For the previous few decades, the photovoltaic (PV) market was dominated by silicon-based solar cells. However, it will transition to PV technology based on flexible solar cells recently because of increasing demand for devices with high flexibility, lightweight, conformability, and bendability. In this review, flexible PVs based on silicone developed using the emerging technology are introduced. The technological limitations of traditional solar cells have been overcome, which will give rise to the new paradigm of solar energy conversion systems and flexible electronic devices. In this review, in terms of flexible PVs, we focus on the materials (substrate and electrode), cell processing techniques, and module fabrication for flexible solar cells beyond silicon.

1. Introduction

As interest in the global warming problem has increased, energy conversion devices have been extensively researched for renewable energy production such as solar energy, wind power, hydroelectric energy, and biomass energy [1–3]. Among them, photovoltaic (PV) devices are considered the most likely candidates as a renewable energy resource that does not emit carbon dioxide, unlike the burning of fossil fuels [4,5]. The PV effect was first discovered by the French Scientist E. Becquerel in 1839 [6]. In accordance with the PV effect, a particular substrate absorbs light and emits electrons or photons that can move freely. The PV effect can be exploited for direct conversion of solar energy into clean, reliable, scalable, and affordable electricity [7,8]. The power from the sun intercepted by the earth is approximately 1.8×10^{11} MW, which is many times greater than the present rate of global energy consumption [9,10]. PV technology is the best method to harness power from natural sunlight. Currently, PV devices such as solar panel cells are typically fabricated on Si-based wafers, which are widely used as both negative- and positive-type semiconductor materials. As PV technology has continued to advance, the possibility of developing flexible PV devices instead of PV devices based on Si wafer substrates has attracted scientific interest [11,12]. However, more advanced technologies must be developed to overcome the current limitations associated with the implementation of flexible PV applications [12,13].

In this review, we describe the recent progress in the field of PV technologies. In addition, we introduce flexible, lightweight, and thin PV devices which go beyond the conventional Si-based devices. Especially, we discuss the materials used and the cell-to-module fabrication methods and then provide a summary with a perspective on the future development and possible technologies involving flexible solar cells.

2. Technology for flexible, lightweight, and thin PV devices

Generally, the processing of flexible PV devices requires a low temperature of approximately 150 °C. In contrast, a high temperature is applied to conventional fabrication processes. Low-temperature processing results in decreased adhesion between the active layer such as the TiO_2 film and substrate and poor film uniformity. To solve these problems, appropriate methods should be developed, and suitable materials should be found [14]. Therefore, state-of-the-art technologies are required for device manufacturing techniques, materials (substrates, electrode, and active), and structures to develop PV devices that are flexible, lightweight, and thin. In this section, we introduce device preparation methods and materials used for developing flexible, lightweight, and ultrathin PV devices.

2.1. Substrate materials

Flexible PV technologies require highly functional materials, compatible processes, and suitable equipment. The highlighting features of flexible PV devices are their low weight and foldability.

* Corresponding author.
E-mail address: bark@gachon.ac.kr (C.W. Bark).

https://doi.org/10.1016/j.mtener.2020.100583
2468-6069/

Appropriate materials as substrates are essential to realize flexible PV devices with stable and excellent performance. The optimal fabrication method to stack layers can be selected according to the substrate type [14,15]. Conventional Si wafers are easily broken by shock and can break when folding by hand because of their single- or poly-crystal structure. However, Si wafers with a thickness of lower than 100 μm could be bendable like paper [16,17]. After growing and cutting Si ingots, the wafers can be made smoother and thinner by mechanical thinning (grinding or lapping) followed by a polishing step such as chemical mechanical polishing, wet etching, or dry etching. However, despite the ultrathin nature of the processed Si wafer, it has limitations for use in flexible PV systems owing to the wafer thickness and high production cost and because it cannot be completely folded [17,18].

To date, metal foil, ultrathin glass, and plastic have been suggested as alternate flexible substrate materials (Table 1). Among them, plastic (polymer) substrates have been widely used for conventional flexible PV devices. Plastic substrates have many advantages, such as good optical transmittance in the visible range, low cost, lightweight, and a simple design. Recently, many studies have focused on the use of plastic materials for flexible circuits [19,20].

As is well known, polymer substrates have poor resilience to high temperature. After annealing for 30 min, an indium tin oxide (ITO) film was deposited onto polyethylene terephthalate (PET) and polyethylene naphthalate (PEN), and its thermal stability was observed, as shown in Fig. 1. The ITO film deposited onto the PET substrate was mechanically constrained on two sides by rigid substrates. As the temperature increased, the ITO/PET films gradually bent. Over 250 °C, the film melted [22,23]. However, with the development of synthesis technologies of polymers, these disadvantages have been overcome. In this section, we discuss various plastic substrates for flexible PV devices. Plastic substrates should meet several conditions: high transmittance, resistance to external shock, stability under chemical exposure, and permeability to water and oxygen. The properties of various substrate materials are summarized in Table 2.

Glass substrates are the most optimal choice for PV devices because of their high transmittance, good absorbance, and emittance of thermal radiation. They are used as front and back layers in solar cells. The front glass layer acts as a pathway for incident light to travel through before reaching the solar cell, where it is ultimately absorbed and generates a current [25]. However, the thickness and dimensional stability of glass substrates are limited. Moreover, they are very weak and can be easily broken when dropped or otherwise subjected to an external impact. However, with the development of glass surface processing technology, ultrathin glass has been developed. Such glass can exhibit high transmittance [24,25]. Fig. 2 shows a solar cell prepared with a bendable glass with a thickness of 100 μm. L represents the

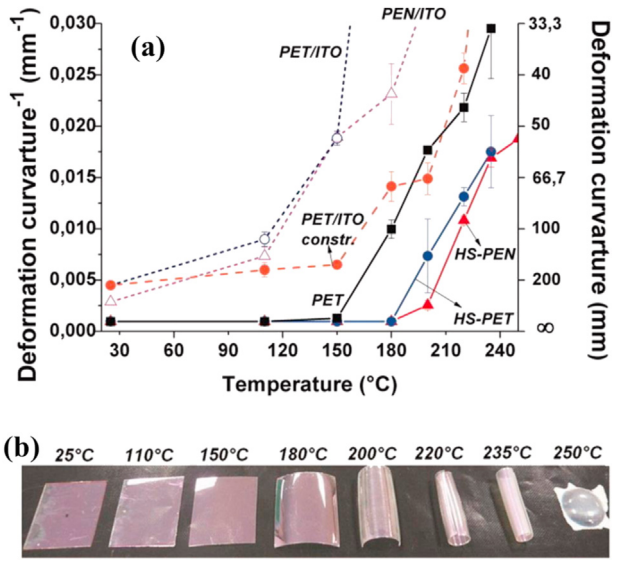

Fig. 1. (a) Deformation of plastic substrates (PET, HS-PET, HS-PEN, PET/ITO, PEN/ITO) in terms of the radius of curvature (and its reciprocal) as a function of treatment temperature. (b) Image of PET/ITO substrates after the thermal treatment. Reproduced with permission from a study by Cole [22]. ITO, indium tin oxide; PET, polyethylene terephthalate; PEN, polyethylene naphthalate.

distance between the two attached edges of the samples, which is 50 mm, as shown in Fig. 2(b).

L was decreased in a stepwise manner to investigate the effect of increasing the curvature of the sample, as shown in Fig. 2(a). At every step, the J–V properties were initially measured on cells 11 and 14 which exhibited similar initial performances and were located in the middle of the sample (region B), where the curvature was maximal. When the curvature reached its maximum point, the sample was returned to the planar state. Fig. 2(b) and (c) show the results of whether the performance evolution induced by curvature is reversible over three bending cycles. The whole operation was successively conducted three times on the same sample to determine whether the evolution of performance induced by curvature was reversible, which would lead to similar performances in the planar state before and after each bending cycle. The sheet resistance slightly increased after bending. However, its values did not return to their initial level at the beginning of the bending cycle because of cell damage by force. After three bending cycles, the light J-V measurements were assessed again. For each of the three points at the surface of the sample before and after the three bending cycles, the performance metrics (V_{OC}, *FF*, and J_{SC}) were observed to have deteriorated under the effect of bending [25].

Table 1
Comparison of plastic, glass, and metal-foil substrates for flexible photovoltaic devices. Reproduced with permission [21].

Materials	Advantages	Disadvantages
Plastic	Foldable and Rollable Good transparency Low cost Lightweight	Poor dimensional stability High water vapor and oxygen gas permeation Low chemical resistance and process temperature
Glass	Conformable Very good transparency Low water vapor and oxygen gas permeation	Easily broken and low mechanical Stability High preparation cost
Metal foil	High process temperature and strong chemical resistance Low water vapor and oxygen gas permeation Good dimensional stability	Very poor transmittance Rough surface Capacitive effect

Table 2
Properties of glass and plastic materials [19–21].

Materials	CTE (ppm/k)	Transmittance (%)	Heat resistance (°C)	Barrier property
Glass	9	90	600	Excellent
PC	70	90	155	Very good
PES	60	89	223	Poor
PET	30	89	78	Poor
PEN	20	88	212	Poor
PI	50	30	340	Poor
PMMA	72	92	80	Poor

CTE, coefficient of thermal expansion; PC, polycarbonate; PES, polyether sulfone; PI, polyimide, PET, polyethylene terephthalate; PEN, polyethylene naphthalate; PMMA, poly(methyl methacrylate) or acrylic.

Polycarbonate (PC) is a low-cost, lightweight, and flexible material, with good transmittance, which is similar to the optical transmittance of glass. However, the main disadvantages of PC are its limitations at high temperatures, its high water permeation, and its poor scratch resistance. Polyether sulfone (PES) is suitable for applications requiring low shrinkage, high tolerances, and small changes over a wide temperature range. PES has excellent thermal resistance of approximately 224 °C, outstanding mechanical/chemical resistance, and good transmittance in the visible range. However, it is yellowish in color and absorbs moisture. PES substrates have a considerably high cost. Polyimide (PI) exhibits high heat-resistance [26]. It has diverse applications in roles demanding rugged organic materials. It can be readily found under the name of Kapton tape, including in our laboratory. As shown in Table 2, PI is more thermally stable than poly(methyl methacrylate) or acrylic (PMMA) (Tg: 80 °C), PET (Tg: 78 °C), and PEN (Tg: 212 °C) substrates. However, the color of normal PI appears light-brown or yellow; thus, it cannot be used for transparent flexible substrates [21–23]. Therefore, other substrate candidates can be used for flexible devices such as PET and PEN. They also have considerably good transmittance and good dimensional stability. During substrate bending, films stacked on the substrate persist for quite a long time. A few years ago, flexible electronic applications used transparent substrates. Recently, colorless PI (CPI) has attracted considerable attention as a flexible substrate [26,27]. Owing to the sufficient thermal stability for high-temperature processing, transparent films such as ITO can be deposited with little changes or damage [28,29].

Fig. 3(a) shows the optical transmittance of ITO films grown on PET and CPI substrates without and with annealing. All samples show an optical transmittance of over 80% in the visible wavelength region between 400 and 800 nm. Fig. 3(d)–(d) show the ITO resistance change on CPI and PET during bending through a fixed bending radius of 5 mm. The ITO film on the CPI substrate showed constant resistance changes during bending, regardless of whether the bending was in the inner or outer direction (Fig. 3(b)). In the case of ITO/PET, the inner bending test showed slight changes in resistance after 10,000 bending cycles; however, the outer bending test showed that the resistance increased by a factor of 1,000 after 2,900 bending cycles. It is assumed that the ITO film on the substrate cracks under tensile stress. In the case of normal and annealed ITO/CPI substrates, both the outer bending tests showed no changes in resistance after 10,000 bending cycles (Fig. 3(c) and (d)), thus demonstrating the higher flexibility of ITO/CPI compared to the ITO/PET sample. PMMA is a strong and lightweight material that offers outstanding clarity, UV stability, surface hardness, and impact resistance. These properties make it ideal for many applications, including fabrication of airplane windshields, skylights, and outdoor windows [21,30,31].

2.2. Electrode materials

All types of devices, including those for both inflexible and flexible applications, have two types of electrodes (positive and negative). Positive electrodes have been fabricated using transparent electrode materials (transparent conducting oxide, [TCO] materials) such as FTO, ITO, and metal-doped ZnO (metal: Al, Ga, In) [32]. FTO is widely used for the development of transparent electrodes in conventional PV applications [33]. However, owing to the high-temperature preparation of FTO, it has a rougher surface than other transparent films and cannot be deposited on polymer substrates [21,22]. If the processing temperature of ITO films exceeds

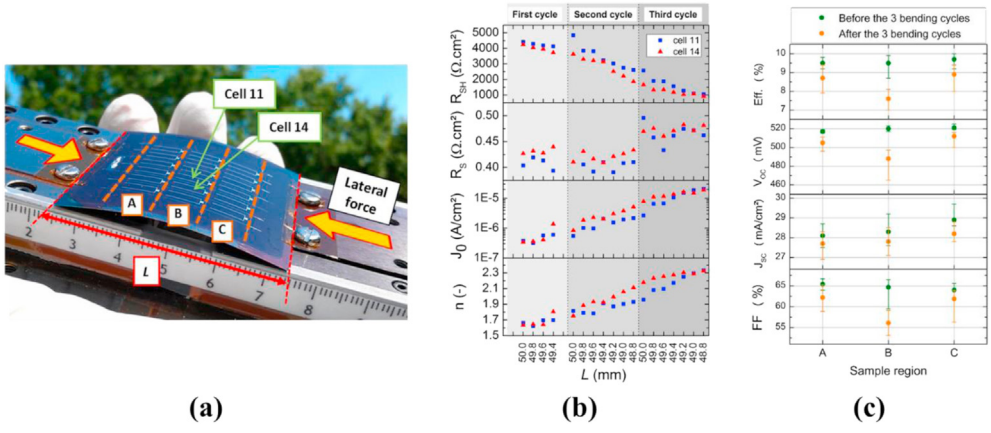

Fig. 2. (a) Photograph of solar cell sample bent by a lateral force, (b) Comparison of electric characteristics drawn from dark J–V measurements of two cells located in the most bent region of the sample during bending, and (c) PV performance from light J–V measurements before and after bending (three times). Reproduced with permission a study by Gerthoffer et al. [24]. PV, photovoltaic.

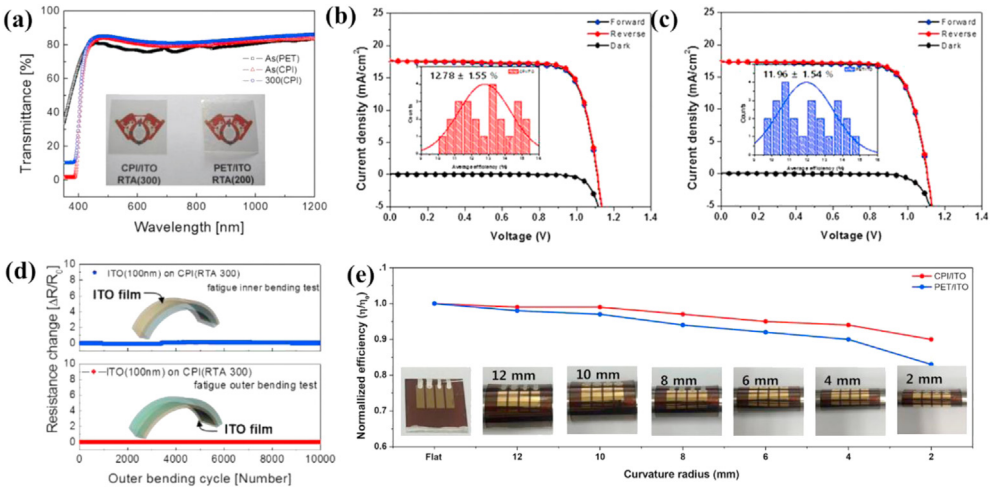

Fig. 3. (a) Optical transmittance of ITO on PET substrate, ITO on CPI substrate, and annealed ITO on CPI substrate; The inset photo shows rapidly annealed ITO on CPI (300 °C) and ITO on PET (200 °C) substrate. (b), (c), and (d) resistance change ratio in the inner and outer of the film during bending; (b) ITO on PET substrate, (c) ITO on CPI substrate, and (d) annealed ITO on CPI substrate. Reproduced with permission from a study by Park et al. [30]. ITO, indium tin oxide; CPI, colorless PI; PET, polyethylene terephthalate.

200 °C, its resistance increases by 1000 times, and it cannot be used as an electrode. Stoichiometric ZnO films exhibit poor electrical properties, such as high resistance. To improve their electrical properties, ZnO films can be doped with Al, Ga, and In [34,35].

In addition, oxide/metal/oxide or metal/oxide multilayer films have been investigated for transparent electrodes [1,37]. Generally, metal materials (Ag, Pt, Cu, and Au) are opaque; however, at film thicknesses below 20 nm, they become clear and transparent. Metal films of nanometer thickness are inserted into intermediate oxide layers [37,38]. Meanwhile, negative electrodes mainly use metal films. The metal materials used as electrodes in the last few decades are mentioned in Table 3. We should consider their cost and performance (conductivity, σ) in terms of device preparation. Representative metals include Ag, Cu, Al, Au, and Ni. In accordance with the information provided in Table 3, suitable metal electrode materials should be selected.

2.3. Cell and module manufacturing

A solar cell is a device that converts sunlight into direct current (DC) electricity via the PV effect. A single solar cell has a voltage of at least 0.5 V at AM 1.5 illumination. In contrast, an electrically charged battery or a conventional battery would require a voltage of at least 15 V or more to be recharged [39]. To generate enough voltage and current for charging the battery, two methods can be used: large-scale active area and high efficiency. However, as the size of the cell increases, the movement distance of the charges (holes and electrodes) collected from the active layer between two electrodes increases, leading to ohmic loss. These problems decrease cell efficiency. Moreover, the efficiency of a unit of solar cell is approximately 26.7% (theoretical efficiency < 29.3%) [40]. A PV module includes numerous unit cells (36–72 cells) wired in parallel to generate useful electricity for performing electronic applications such as increasing current with high voltage. Conventional PV modules are classified as amorphous silicon, crystal silicon, and thin-film modules [41]. Silicon-based solar cells are non-flexible or exhibit slight bendability. As the thickness of the silicon wafer reduces (<5–50 μm), the cell could become flexible and bendable. Compared with thin-film solar cells (Copper Indium Gallium Selenide (CIGS) and Gallium Arsenide (GaAs)), amorphous silicon and crystalline silicon (single or polycrystalline) solar cells have been developed in limited fields. Because the PV module is encapsulated within an assembly with the PV unit solar cell and protective layers to maintain stable performance against air, vapor, high temperature, and moisture, the prepared PV module could continue to generate electricity for over 20 years if it does not undergo internal breakdown [39,41].

Even though the PV module could be perfectly designed and prepared for flexible solar cells, the total reduction in efficiency of PV modules to collect the generated energy cannot be avoided in all. Therefore, to overcome these problems, many research groups have been attempting to develop new technologies. Most importantly, the active area must be increased. The efficiency of recent emerging PV devices such as organic solar cells (OSCs), perovskite solar cell (PSCs), and dye-sensitized solar cells (DSSCs) is ideal values measured from the unit cell of area ~1 cm^2 in the laboratory [25,42]. PV modules with a much larger size than 100 cm^2 are required to store enough power energy to operate electronic applications. Module components in series connections are the best choice to increase voltage while maintaining DC in the unit and connected cells.

Table 3
Comparison of candidate materials for metal electrodes. Reproduced with permission in a study by Wang et al. [36].

Materials	σ_{dc} (Sm^{-1}@20 °C)	Cost (US dollar per kg)	Normalized conductive/cost ratio
Ag	6.30×10^7	510	0.014
Cu	5.96×10^7	6.7	1
Au	4.10×10^7	40070	0.000011
Al	3.50×10^7	2.0	2
Ni	1.43×10^7	11.1	0.14
Pd	1.0×10^7	32408	0.000035
Pt	9.43×10^7	28260	0.000037

Fig. 4(a) shows a cross-section image of a monolithically interconnected thin-film solar module. The module's performances depend on the internal resistances. The sheet resistances in modules connected in series represent the top electrode ($R_{s,top}$), bottom electrode ($R_{s,bottom}$), and the interconnect resistance (R_{int}) in the P2 line contact between the top electrode and bottom electrode. The area of P1 to P3 (area with = L) is the non-photogenerated section (dead area), which usually leads to energy loss in the modules. We can evaluate the active area of the designated modules from the geometric fill factor (GFF) as follows [44]:

$$GFF = (1 - \text{dead area/total area}) \times 100\ (\%)$$

where L is the active length which depends on the value of GFF, $R_{s,top}$, and $R_{s,bottom}$.

The DSSC module (DSM) can be designed in four types: monolithic, parallel grid, Z-type, and W-type, as shown in Fig. 4(b). The monolithic type represents series interconnections, and inexpensive carbon black is used instead of platinum. Compared with other designs, the production cost can be reduced by 20–30%. DSMs comprising six cells of 4.7 × 0.7 cm^2 with an active area of 21 cm^2 have an efficiency of 5.3% (V_{OC} 3.90 V, I_{SC} 28.55 mA, and FF 1.3). Their active area ratio to total area can reach over 90% [45].

The parallel grid connection type is used to improve short-current density (J_{SC}). In parallel connections, the charge is collected in two ways between the side area in contact with the FTO electrode and metal grids (Ag, Ni, Cu Al, and Au). Späth et al. [43] reported the successful fabrication of 27 upscale up cells (5 cm^2–100 cm^2) with a power conversion efficiency of 4.3%

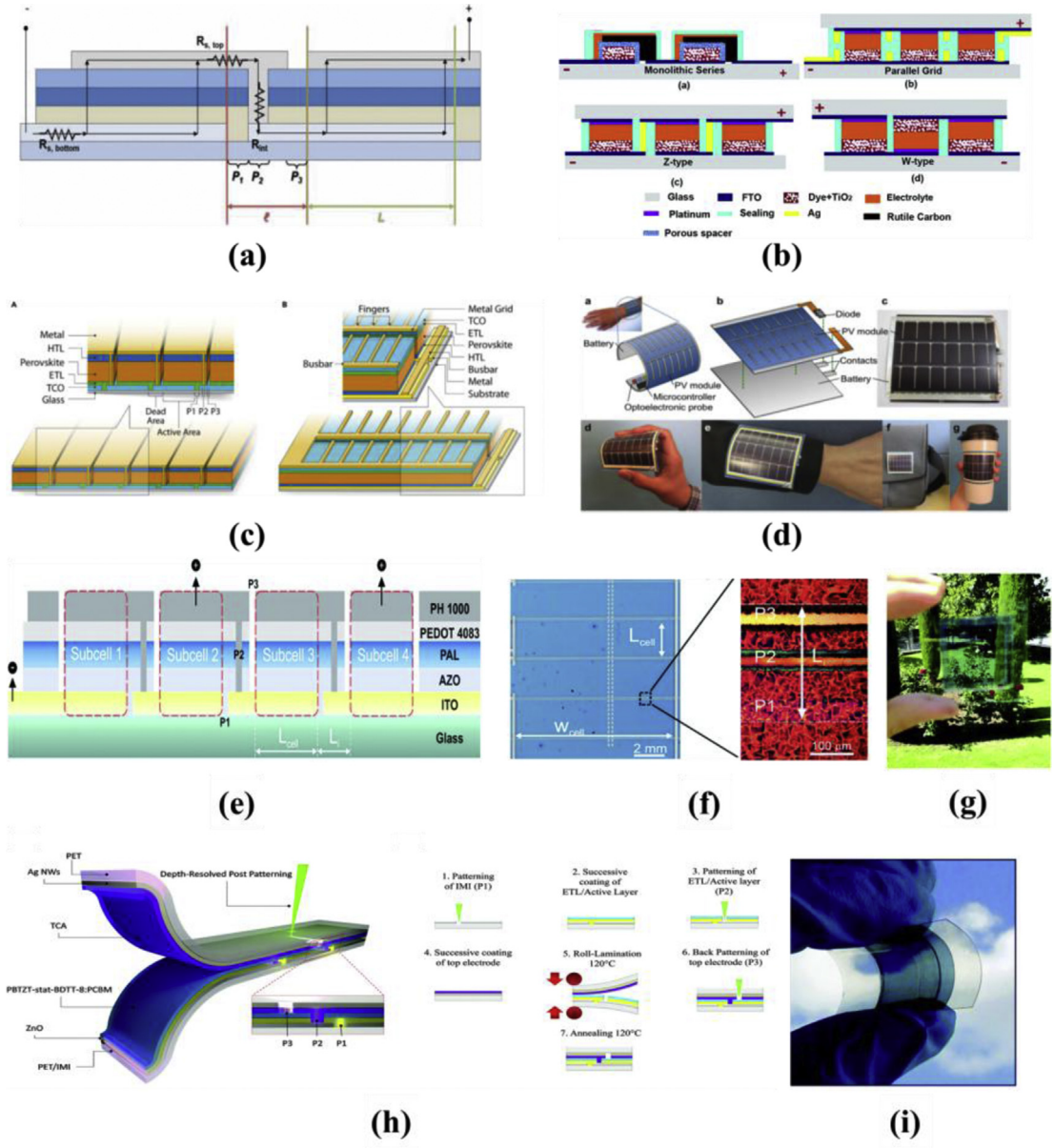

Fig. 4. (a) Cross-section of a thin-film solar module with monolithic integration. Reproduced with permission from a study by Lucera et al. [44]. (b) Schematic of different types of DSMs with series connections: monolithic, parallel grid, Z-type, and W-type. Reproduced with permission from a study by Fakharuddin et al. [45]. (c) Schematics of monolithic- and grid-interconnected PSMs [46]. (d) various applications related with a flexible module. Reproduced with permission from a study by Ostfeld et al. [47]. (e), (f), and (g) General schemes of the (a) cross-section, top view and photograph of sample of laser-patterned modules. Reproduced with permission from a study by Pascual-San-José et al. [51]. (h) Schematic structure and fabrication processing via laser pattering of organic solar cell and module and (i) photograph of module monolithically interconnected. Reproduced with permission from a study by Spyropoulos et al. [52]. DSM, DSSC module; PSMs, perovskite solar modules.

(standard deviation: 7) even though the active area ratio is low 68 cm^2.

Z-type and W-type interconnections use a vertical metallic conductor. Toyoda et al. [48] developed a 64 cell unit (10 × 10 cm^2) prepared on the large panel and showed that the performances were stable for six months as the corrosion of the metal electrode was delayed. Sastrawan et al. [49] prepared DSMs with an area of 10 × 10 cm^2 (an active area of 680 cm^2) which exhibited an efficiency of 3.5%, V_{OC} of 20 V, I_{SC} of 168 mA, and FF of 0.53. Jun et al. [50] fabricated DSMs (10 × 10 cm^2) that exhibited conversion performances with an efficiency of 6.6%, V_{OC} of 8 V, J_{SC} of 1.23 mA cm^2, and F.F. of 0.67. Z-type DSMs have a considerably high voltage; however, they have limitations in terms of the relatively low active areas [45]. DSMs with W-type architecture have attracted attention to solve this problem. Unlike the Z-type module, each cell in the W-type module is above and below the neighboring cells, as shown in Fig. 4(b). Compared with the Z-type design, the architecture has more effect on the higher F.F. and J_{SC} of cells.

Modules with PSCs can be assembled with monolithic- and grid-interconnection types (Fig. 4 (C)). In the case of monolithic-interconnection type, the series connection is the most simple and commonly employed module fabrication method. P1, P2, and P3 are in the module (Fig. 4(a)), and the GFF is relatively narrow at approximately 95%.

Pascual-San-José et al. [51] reported monolithically combined semitransparent organic cells (over 30%), as illustrated in Fig. 4(f) and (g). They employed a pulsed laser with an excitation of 1064 nm and a minimum pulse width of 1 μs at repetition rates of up to 200 kHz for laser patterning in modules. The solar cell devices were fabricated under ambient conditions (heating annealing temperature < 80 °C) and were characterized by an inverted structure with glass substrate/ITO/AZO(electron transport layer; ETL)/PBTZT-stat-BDTT-8 (photoactive layer; PAL)/poly(3,4-ethylenedioxythiophene):poly(styrenesulfonate) [PEDOT:PSS] (hole transporting layer; HTL)/PH1000(top electrode). The PH1000-based electrode was used in place of the Ag metal electrode, and PH1000 was formed using the solution process. The laser patterning process was performed as follows: P1 on ITO, P2 and PEDOT coating and P3 after top electrode (PH1000) was coated on the active layers, as depicted in Fig. 4(e). The modules comprised 2 or 4 interconnected unit cells connected in series and exhibited power conversion efficiencies in the range of over 4% with an active area above 1 cm^2.

Spyropoulos et al. [52] prepared the organic and perovskite solar modules on the PET film using an ultra-fast laser-patterning technique. All the unit solar cells were fabricated on the PET substrate using the doctor blading method. The monolithic interconnected modules (MIMs) were fabricated using the subcells through the laser scribing process, which was performed in three steps, namely, P1, P2, and P3, as depicted in Fig. 4(h). The module's power conversion efficiencies increased from 5.3% to 9.8% after the subcells were interconnected. Moreover, fill factors of over 90% were achieved.

Compared with the monolithic interconnection type, the GFF of the grid-interconnection type is lower because a metal grid is placed on each cell. The grid-interconnection module has the advantage that it can improve current over a large area (25 cm^2) of the unit cell to prevent a reduction in the F.F., thus allowing the upscaling of the active size of the module. However, the energy conversion performance loss is caused by the reduction of absorbance area shading with a coating over the grid metal lines drawing in each cell.

In Fig. 4(d), when the PV module is combined with functional units such as a battery and Schottky diodes, such modules can be used to develop various wearable electronics being flexed in the hand, a sleeve in outer cloth, bag, and mug tumbler. As the technology for fabricating improved PV modules is developing, many challenges will be highlighted in the future.

3. Beyond Si-based flexible PVs

Since Chapin et al. [53] reported silicon-based p−n junction photocells with an efficiency of 6% for photon energy conversion systems in 1954, numerous PV technologies have been developed to improve this performance. Until now, three generations of PV cell technologies have been developed for application in solar cells. However, first-generation silicon-based solar cells (mono- and polycrystalline silicon wafer) have dominated over 90% of the PV market due to relative abundant raw materials such as silicon (Si), even though the maximum theoretical energy conversion efficiency of PV devices is limited to 33% [54]. Moreover, silicon-based solar cells have a disadvantage that they have a relatively weak absorbance for long wavelengths from sunlight, and the thick (100−500 μm) silicon substrate cannot be bended and is opaque. Silicon-based solar cells have a limited potential for application in flexible PVs because of their drawbacks [55]. Thus, now we introduce flexible PV technology beyond silicon.

3.1. Flexible OSCs

Flexible OSCs have received increasing attention for use in portable electronics, wearable electronic textiles, or roll-type applications because their lightweight and mechanical flexibility are compatible with the requirements of curved surfaces and soft materials [56−61]. Because of their rapid development, the efficiency of OSCs has reached as high as 17% for tandem cells and 14% for single cells on rigid glass substrates [62−64]. To date, the power conversion efficiency (PCE) of flexible OSCs is relatively lower than that of cells on rigid glass substrates, which is approximately 15% on ITO glass [65−67]. Beginning with flexible OSCs with a PCE of 1.5% introduced by Kaltenbrunner in 2012 [55], their efficiency has since improved rapidly to 12.5%, as reported by Xiong in 2019 for non-fullerene OSCs [66]. To enhance the efficiency of flexible OSCs, different flexible substrates must be investigated to replace ITO, such as carbon-based materials [68−70], metallic nanostructures [71−73], or hybrid composite electrodes [74]. In the following sections, we review the development of flexible OSCs based on conventional ITO electrodes, conducting polymer transparent electrodes, metal-based transparent electrodes, and carbon materials.

3.1.1. Conventional ITO-based electrodes

Thin films of ITO have been widely used in numerous electronic and optoelectronic applications as transparent electrodes in solar cells because of their unique characteristics, such as high electrical conductivity and high optical transmittance in the visible region, high infrared reflectance, and excellent substrate adhesion [75−77]. However, the raw indium material used in ITO exhibits certain disadvantages in terms of availability and cost [78]. Moreover, it is incompatible with plastic-based substrates because of its brittleness during bending. Despite these problems, numerous studies have reported flexible solar cells developed using flexible ITO electrodes. Flexible OSCs using ZnO nanoparticles on ITO-plastic substrates were developed in 2008 and exhibited a 3.3% efficiency, compared with a PCE of 3.61% achieved by rigid OSCs [79]. This inverted configuration exhibited higher stability under ambient conditions after 40 days because of the enhanced stability of the poly(3,4-ethylenedioxythiophene):poly(styrenesulfonate)/Ag interface, although the conditional structure showed significant degradation after four days. The efficiency of flexible OSCs was

slightly enhanced because of the electron-selective layer of ZnO grown using atomic layer deposition (ALD) under a deposition temperature of 80 °C [80]. The thickness of the ZnO thin-film was 0–72 nm, with the highest efficiency achieved for 36 nm, and the efficiency gradually decreased as the ZnO thickness increased. The processing temperature is an important issue for the fabrication of flexible solar cells because the active layer of flexible OSCs requires thermal annealing at over 150 °C, which is incompatible with manufacturing using plastic substrates. To resolve these heat-related problems, an ideal PAL was synthesized in 2012 using an additive without thermal annealing to achieve high efficiency of 6% [81]. da Silva [82] fabricated inverted transparent flexible OSCs with an efficiency of 6.87% by adding an 18 nm thick polyaniline (PANI) layer as an anode buffer layer between the PAL and the top anode in transparent flexible OSCs. Zhao [83] fabricated low-temperature–processed high-efficiency flexible OSCs using PET/ITO, based on the low bandgaps of the semiconducting polymers thieno [3,4-b] thiophene/benzodithiophene (PTB7) and [6,6]-phenyl C71-butyric acid methyl ester (PC71BM) to achieve a PCE of 8.7%, compared with the efficiency of 9.2% achieved using an ITO/glass substrate.

Fig. 5 shows (a) the optical transmittance of the PET/ITO (40 Ω/sq) and glass/ITO (15 Ω/sq) substrates, (b) J–V characteristics of the flexible OSCs with a PCE of 8.71%, and (c) an image of flexible OSCs annealed at different temperatures (30, 80, 110, 140, 155, and 170 °C) for 10 min. Moreover, a high-performance flexible tandem OSC using a PEN/ITO flexible electrode and a tetrabutylammonium iodide (TBAI)–doped cross-linked azidofullerene derivative PCBN3 film as the ETL delivered a high PCE of 9.2% in 2015 [84]. Although ITO-based flexible electrodes have been used in flexible OSCs by spin-coating or R2R technologies, the PCE of the scaled-up flexible solar cells is much lower than that of other flexible electrodes. Thus, the challenge in enhancing the efficiency of large-area flexible OSCs used with ITO electrodes lies in the development of low-resistance and highly mechanically stable flexible electrodes.

3.1.2. Carbon-based electrodes

3.1.2.1. Graphene. Graphene has been investigated as a promising replacement for ITO materials because of its inherent high chemical and thermal stability, excellent electrical and optical properties, potentially low-cost processing, and low contact resistance with organic materials in flexible OSCs [85,86]. Graphene can be deposited using various techniques such as chemical synthesis, chemical vapor deposition (CVD), or reduction of graphite oxide (rGO). Among them, CVD- and rGO-based techniques are more appropriate for graphene-based flexible OSCs. Because of the attractive properties of graphene, several articles on graphene-based OSCs have been published involving electrode applications [87–92]. However, the efficiency of graphene-based flexible OSCs is low compared with that of conventional devices. Yin [93] reported a low efficiency of 0.79% because of the low optical transmittance and high sheet resistance resulting from the rGO method, in which films were transferred onto PET substrates.

Fig. 6(a) illustrates the layered structure and energy levels of a flexible rGO/PEDOT:PSS/P3HT:PCBM/TiO_2/Al solar cell, with rGO as the transparent electrode. To enhance the performance of graphene-based flexible OSCs, the sheet resistance of the graphene film must be reduced. In one study, single-walled carbon nanotubes (SWCNTs) were used to control the properties of the electrode. Using this technique, inverted flexible OSCs based on P3HT/PCBM

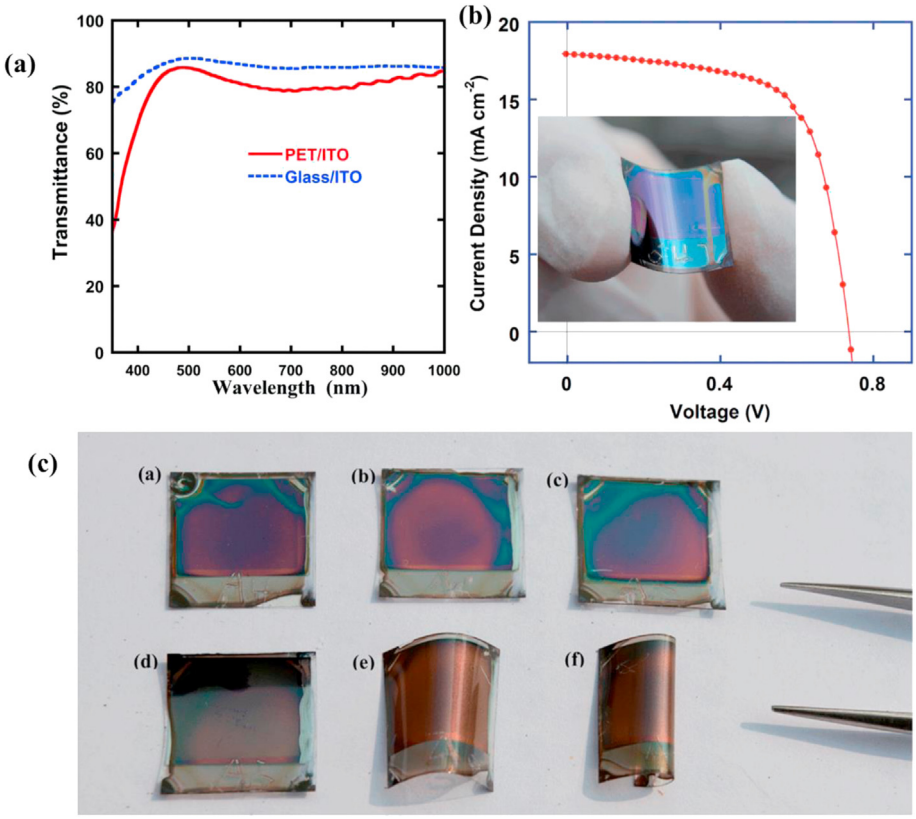

Fig. 5. (a) Optical transmittance of the PET/ITO (40 ohn/sq) and glass/ITO (15 Ω/sq) substrates. (b) J–V characteristics of flexible OSCs with a PCE of 8.709%. (c) Image of flexible OSCs annealed at different temperatures (30, 80, 110, 140, 155, and 170 °C) for 10 min. Reproduced with permission from a study by Zhao et al. [83]. ITO, indium tin oxide; PET, polyethylene terephthalate; OSCs, organic solar cells.

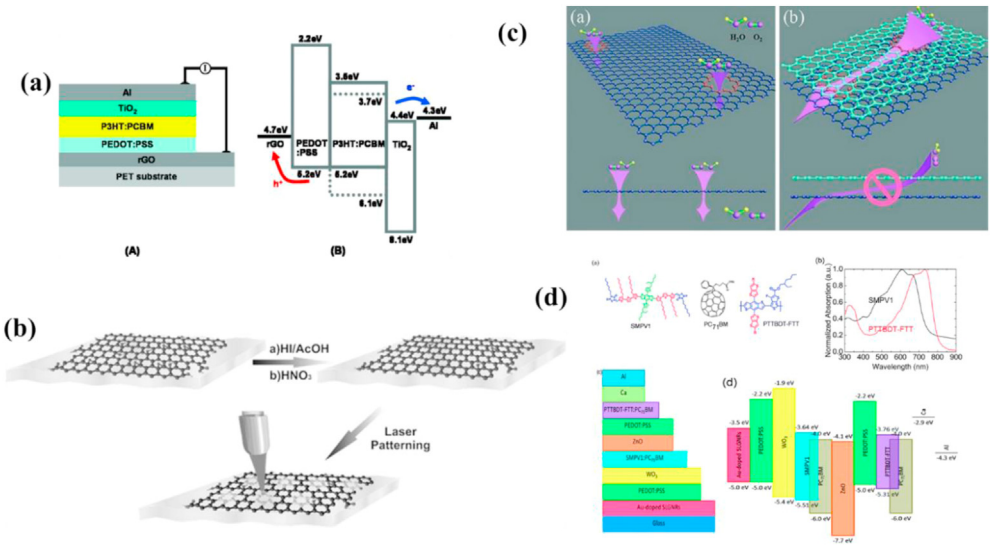

Fig. 6. (a) Schematic representation of layer structure and energy levels for flexible OSCs. Reproduced with permission a study by Yin et al. [93]. (b) Schematic of rGO mesh electrodes preparation. Reproduced with permission from a study by Konios et al. [94]. (c) Single- and double-layer graphene films acting as H2O and O2 barriers. Reproduced with permission from a study by Li et al. [95]. (d) Molecular structures of SMPV1, PTTBDT-FTT, and PC71BM; absorption spectra of SMPV1 (black) and PTTBDT-FTT (red) thin films; device structure; energy levels of the ITO-free tandem solar cell. Reproduced with permission from a study by Liu et al. [96]. ITO, indium tin oxide; OSCs, organic solar cells; rGO, reduction of graphite oxide.

achieved an efficiency of 1.27%, and an efficiency of 3.05% was obtained later by using rGO as the bottom transparent electrode (BTE) for improved optical transmittance [94]. However, the high sheet resistance of the rGO films limits their application in flexible OSCs. Fig. 6(b) shows a schematic diagram of the fabrication of the rGO. In a separate study, CVD was used to synthesize high-quality and large-area graphene films as electrodes with low sheet resistance and better conducting properties [95]. Liu et al. [96] fabricated flexible OSCs with PEDOT:PSS/Ag films, and the graphene top electrodes exhibited a PCE of 3.17% (refer Fig. 6(c)). However, flexible OSCs must be protected from moisture or oxygen permeation for stable operation because of the top two-layer graphene electrodes [84]. Yusoff et al. [97] investigated Au-doped single-layer graphene nanoribbons as the conducting electrode material for ITO-free tandem polymer solar cells with a PCE of 8.48%, as shown in Fig. 6(d).

3.1.2.2. Carbon nanotubes. SWCNTs have attracted attention for replacing ITO in flexible OSCs [98]. They have demonstrated potential in flexible devices because of their transparency, good electrical properties, high flexibility, and low-temperature processing. Carbon nanotubes (CNTs) have low sheet resistance because of the low transmittance induced by the high-density CNT film [99]. Rowell et al. [100] fabricated flexible transparent conducting electrodes by printing SCWNT networks on plastic. They achieved a PCE of 2.5% (AM1.5G) using a PET/SWNTs/PEDOT:PSS/P3HT:PCBM/Al device structure, compared with the 3.0% achieved using a conventional ITO-based structure. Fig. 7(a) indicates that a transmittance of 85% was achieved in the visible region for an SWCNT film with a sheet resistance of 200 Ω/sq, compared with the transparency of ITO on glass with a sheet resistance of 15 Ω/sq. CNT electrodes were prepared by CVD to obtain different transparencies by varying the thickness of the SWCNT film [101]. Later, Jeon fabricated SWCNT films doped with MoOx as electron-blocking electrodes by direct and dry deposition methods [102]. The resulting flexible OSCs achieved an efficiency of 3.91% under a severe cyclic flex test (refer Fig. 7(b)). Although graphene and CNTs have been widely used in flexible OSCs, certain challenges such as low performance, low electrical conductivity, low stability, and mass-production issues remain to be solved for their practical use in flexible OSCs.

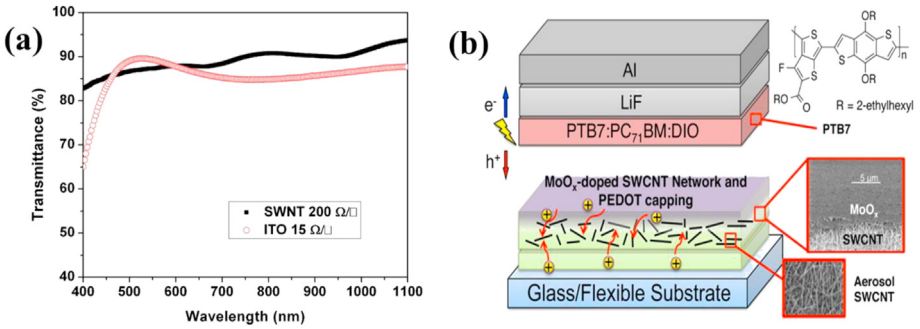

Fig. 7. (a) Transparency of a 30-nm-thick nanotube film versus ITO on the glass. Reproduced with permission a study by Rowell et al. [100]. (b) Configurations of flexible OSCs (glass or flexible substrate/MoOx/SWCNT/MoOx/PEDOT:PSS/PTB7:PC71BM/LiF/Al). Reproduced with permission a study by Jeon et al. [102]. ITO, indium tin oxide; OSCs, organic solar cells; SWCNT, single-walled carbon nanotubes; PEDOT, poly(3,4-ethylenedioxythiophene); PSS, poly(styrenesulfonate).

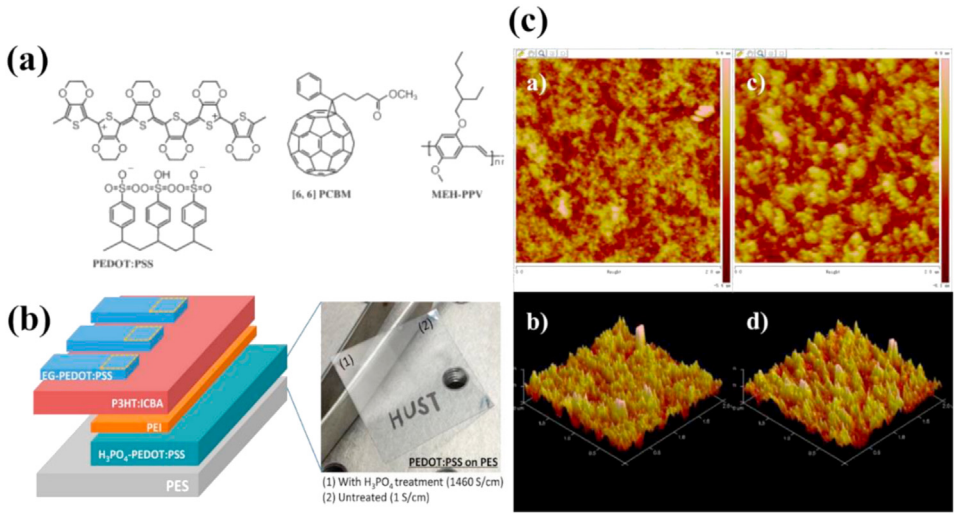

Fig. 8. (a) Molecular structures of PEDOT:PSS, MEH-PPV, and PCBM. Reproduced with permission a study by Jeon et al. [102]. (b) Structure of a flexible all-plastic solar cell. Reproduced with permission from a study by Meng et al. [104], (c) 3D AFM images of pristine PEDOT:PSS film and H_3PO_4 treated PH1000 film. Reproduced with permission from a study by Meng et al [104]. PEDOT, poly(3,4-ethylenedioxythiophene); PSS, poly(styrenesulfonate); PCBM, phenyl-C61-butyric acid methyl ester.

3.1.3. Conducting polymer-based electrodes

Conducting polymers have been investigated for use in flexible OSCs because of their intrinsic flexibility and compatibility with mass-production techniques. Thin films of PEDOT:PSS (as shown in Fig. 8(a)) were first fabricated to replace ITO as BTEs in OSCs [103]. However, the resistance of the ITO anode was 20 Ω/sq, whereas the normal PEDOT:PSS resistance was 1.5×10^5 Ω/sq, which was reduced by treatment with glycerol PEDOT:PSS:G (1.3×10^3 Ω/sq) and sorbitol PEDOT:PSS:S (1.0×10^3 Ω/sq). The MEH-PPV/PCBM based devices achieved a PCE of 0.36%, compared with 0.46% for ITO-based PV cells. Meng reported the use of a H_3PO_4 treatment to enhance the PEDOT:PSS conductivity to 1460 S/cm on plastic substrates [104].

The flexible, all-plastic solar cells (PES/H_3PO_4-treated PEDOT:PSS/PEI/P3HT:ICBA/EG-PEDOT:PSS (shown in Fig. 8(b)), exhibited an open-circuit voltage of 0.84 V, a F.F. of 0.60, and a PCE of 3.3% under 100 mW/cm^2. However, the sheet resistance of H_3PO_4−PEDOT:PSS films on PES substrates is relatively higher (approximately 120 Ω/sq) compared with that of films on glass substrates. The difference in surface roughness (see Fig. 8(c)) limited its further application in flexible devices.

The conductivity of the PEDOT:PSS film was significantly enhanced through a co-solvent treatment from 0.2 S cm^{-1} to more than 100 S cm^{-1} by Xia and Ouyang [105]. The cosolvent-treated PEDOT:PSS films exhibited a PV efficiency of approximately 3% under 1.5G illumination. Later, in 2016, mild acids were used to increase the conductivity and enhance stability in an ambient atmosphere of flexible OSCs by transfer-printed PEDOT:PSS electrodes [106]. The acid-treated flexible OSCs achieved 84% of the PCE achieved by rigid glass OSCs. Flexible OSCs have been successfully fabricated using conducting polymers as electrodes. However, PEDOT:PSS electrodes exhibit medium transparency and an acidic and hygroscopic nature, resulting in device degradation, which may limit their further application toward high-efficiency flexible OSCs.

3.1.4. Ag nanowire-based electrodes

Silver nanowires (AgNWs) have been reported to form thin-film networks on flexible substrates which can then act as transparent electrodes owing to their high transmittance, inherent low resistivity, and good mechanical flexibility, which make them suitable for technologies such as R2R, transfer printing, or air spraying [72,107,108]. Lim et al. [109] fabricated flexible AgNW layers on a PET substrate as electrodes using a simple brush-painting method that achieved a 3.23% PCE, compared with 3.34% for ITO/glass. The AgNW network electrodes had a low sheet resistance of 38.7 Ω/sq and high diffusive transmittance of 87.62%. A transfer method was investigated to transfer AgNWs films onto PET substrates. However, this method required special treatment because of poor adhesion between the PET substrates and the AgNW films [108]. Song et al. [110] fabricated highly efficient and bendable OSCs using solution-processed AgNW electrodes. These flexible OSCs exhibited a PCE of 5.02%, with a minor reduction after 1000 bending cycles (radius of 1.5 mm). Flexible OSCs fabricated from PET/AgNWs/PFN electrodes under a low-temperature solution process achieved PCE of 6.13%, with a reduction of 10% after bending the cell to 5 mm [111]. Recently, a PCE of 8.75% was achieved on a flexible PET by reducing the surface roughness of AgNW electrodes [112].

Fig. 9(a) shows a schematic diagram of the fabrication of a AgNW electrode using CIP to fabricate AgNW junctions on a suspended substrate. A highly efficient flexible OSC was developed based on hybrid electrodes comprising AgNW/PET films with different sheet resistances and PEDOT:PSS PH1000 (refer Fig. 9(b)) doped with various amounts of ethylene glycol (EG) to enhance film conductivity [113]. The film retained approximately 90% of the original PCE after 1000 bending cycles and over 75% of the original PCE after complete folding. Dong et al. [114] fabricated flexible non-fullerene OSCs (AgNWs@PI/ZnO/active layer/MoO_3/Ag) with a PCE of up to 11.6% in 2019 (Fig. 9(c)). They demonstrated that AgNWs embedded in PI substrates improved the efficiency of non-fullerene OSCs, and PI substrates could tolerate temperatures of over 300 °C. Therefore, AgNW-based flexible OSCs have demonstrated several advantages, such as good flexibility and conductivity, for their practical application in flexible devices.

3.2. Flexible PSCs

Perovskite represents a group of materials that have the general formulation ABX_3, where A is a 12-fold 'X'-coordinated cation, and B is a 6-fold 'X'-coordinated cation. Most inorganic perovskites (mostly oxides) encompass an array of physical properties such as ferro-, piezo-, and pyro-electricity [115,116]. The range of electrical properties from dielectric to superconductivity exhibited by

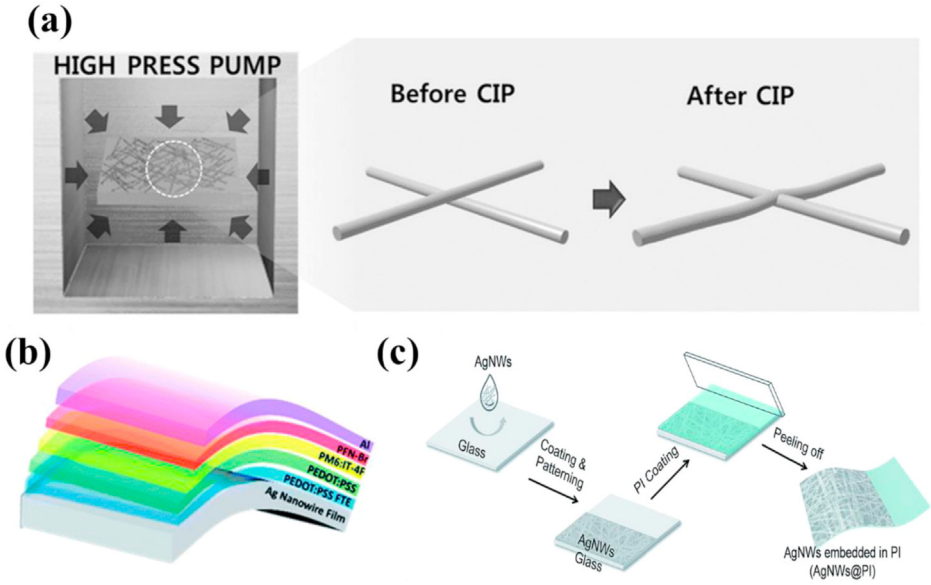

Fig. 9. Schematic of the fabrication of a silver nanowire (AgNW) electrode using cold isostatic pressing (CIP) for AgNW junctions on a suspended substrate. Reproduced with permission from a study by Seo et al. [112]. (b) Structure of flexible OSCs based on AgNW film plastic substrates in water. Reproduced with permission from a study by Lei et al. [113]. (c) Schematic of the preparation of flexible AgNWs@PI. Reproduced with permission from a study by Dong et al. [114].

perovskites can be considered as the widest range of physical properties exhibited by a single material. Recently, organic-inorganic halide perovskites have shown remarkable performance as semiconductors applied in light-emitting diodes and thin-film transistors, as first reported by Schmid and Gebauer [117] and Mitzi [118], respectively. A is typically methyl-ammonium (CH_3NH^{3+}) or formamidine ($CH_3CH_2NH^{3+}$), B is a divalent metal ion such as Pb^{2+} or Sn^{2+}, and X consists of halide anions (I^-, Br^-, Cl^-), which bond to both A and B. In terms of solar cells, an organic-inorganic perovskite, specifically $CH_3NH_3PbI_3$, was first applied in a solar cell as the sensitizer in a liquid-electrolyt—-based DSSC structure in 2009 by Kojima et al. [119]. Although a low efficiency of 3.8% was achieved, they introduced a new class of PV materials. The accumulated research revealed the advantages of perovskite materials, including a desirable bandgap (1.55 eV) [120], high adsorption coefficient (10^3 cm^{-1}), low binding energy (allowing a film of less than 500 nm thickness to collect most of the incident light) [116], a long charge diffusion length (up to 175 μm for single crystals) [121], and other advantages, making the organic-inorganic PSCs promising candidates in the PV field. Within a short period of time, the PCE of PSCs rapidly increased to as high as 23.3%, which is the highest efficiency compared with all other thin-film solar cells [122]. As a subarea of PSCs, interest in flexible PSCs is increasing rapidly to meet the demands of portable electronics, shaped display devices, and wearable electronic textiles. Moreover, based on R2R or web technology, flexible PSCs are compatible with mass- and rapid-production processes, which makes them less expensive than their glass substrate counterparts. However, flexible PSCs commonly use a metal or polymer substrate, which can strongly affect the required device processing procedures. For example, polymer substrates for flexible PSCs cannot withstand high temperatures (well below 150 °C), whereas high-temperature processes are commonly used to fabricate films on glass substrates. Therefore, in developing flexible PSCs, research has mostly focused on alternative materials and/or low-temperature processes. In this part of the review, flexible PSCs will be addressed from two main viewpoints: flexible PSCs based on polymer substrates and flexible PSCs based on metal foils.

3.2.1. Polymer substrate

The commonly used materials in flexible PSCs of this class are PET and PEN. In some studies, these substrates are typically coated with a TCO such as ITO [123], indium zinc oxide (IZO) [124], or Al-doped ZnO (AZO) [125] because of their transparency and conductivity. However, polymeric substrates/TCOs have some issues. First, as a brittle material, TCO can be damaged or destroyed during bending, leading to increased substrate resistance. Second, the polymer material/ITO has reduced chemical resistance compared with glass substrate/TCO.

3.2.1.1. TCO electrode

3.2.1.1.1. Conventional n—i—p architecture. For this structure, the layer deposited on the TCO is an n-type layer (or ETL), which allows extraction of photogenerated electrons from the perovskite layer, transports them to the TCO, and avoids recombination between the TCO and perovskite using a compact layer. The suitable candidates for ETLs are TiO_2, ZnO, and SnO_2 because of their appropriate energy levels. Among them, SnO_2 has the highest electron mobility and the largest bandgap and is a UV-stable material [126–128]. However, ZnO was chosen to fabricate a flexible PSC in the beginning because the production process requires a lower temperature than that required for other candidates [129], even though the efficiency was limited to 2.62% on PET (versus 8.9% on glass). To improve the performance of flexible PSCs based on ZnO_2, sputtering of a ZnO layer onto flexible glass was also investigated. Presently, the record efficiency of devices employing ZnO is 15.5%, which is based on the PEN/ITO/ZnO/$MAPbI_2$/PTAA/Au structure [130]. One of the drawbacks of using ZnO is its low stability. ZnO can have an adverse effect on the perovskite layer because it can rapidly reduce its efficiency [131]. To overcome this issue, an effective temperature procedure for TiO_2 should be applied. Various methods have been investigated, including sputtering, ALD, e-beam evaporation, and solution processing. To date, the best device among flexible PSCs using TiO_2 in which radio frequency (RF) magnetron sputtering of TiO_2 was performed onto PET/ITO exhibited an efficiency of 15.88% [132]. In terms of SnO_2, plasma-enhanced ALD technology was used to fabricate a thin layer of SnO_2 with an efficiency of 17.08% [133].

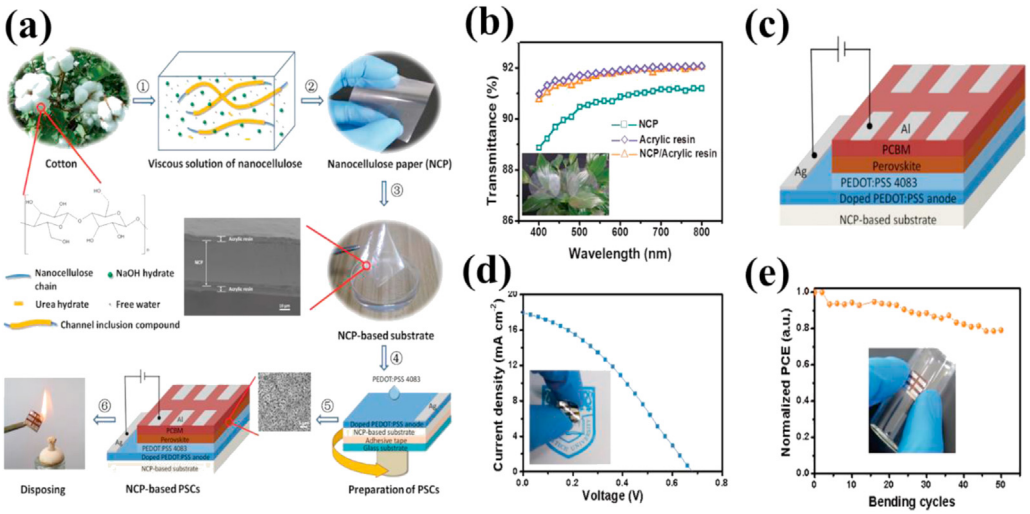

Fig. 10. (a) Preparation process of NCP-based substrate and NCP-based PSCs, (b) schematic device structure of NCP-based PSCs, (c) current density-voltage (J–V) characterization of NCP-based PSCs, (d) normalized PCE-bending cycles characterization during bending state by hand on a glass bottle with a diameter of 15 mm, and (e) optical transmittance of NCP and NCP-based substrate with a coating of acrylic resin. Reproduced with permission a study by Gao et al. [166]. PSCs, perovskite solar cells.

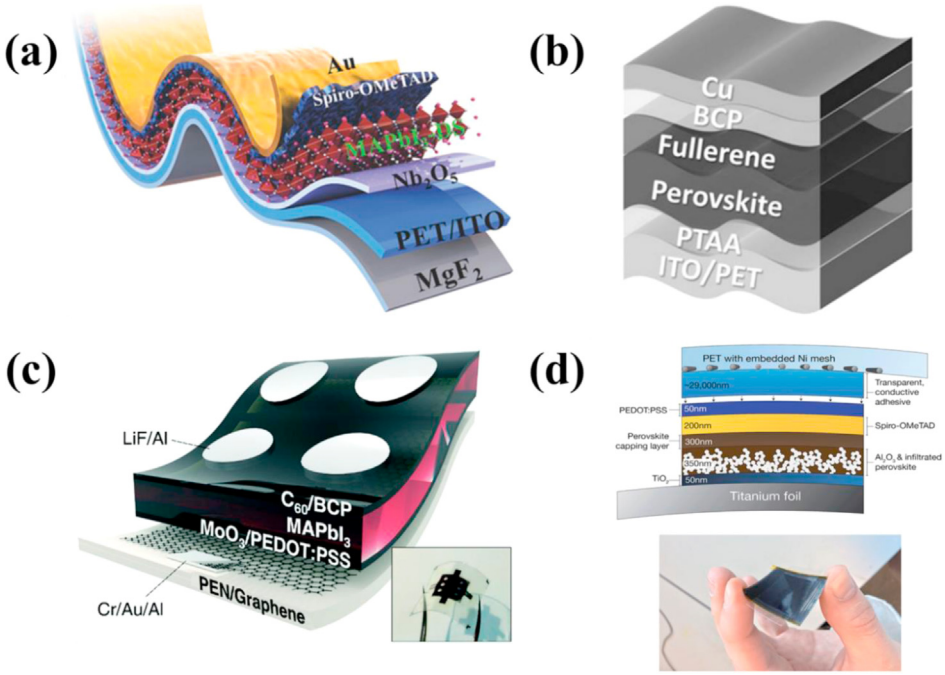

Fig. 11. (a) Nb_2O_5 was exploited as the ETL for flexible PSCs. Reproduced with a study by Feng et al. [134]. (b) PTAA used as HTL in inverted architecture. Reproduced with permission by a study by Bi et al. [140]. (c) Flexible PSCs based on polymer substrate without TCO. Reproduced with permission [147]. (d) Flexible PSCs based on the metal substrate. Reproduced with permission from a study by Lin et al. [170]. PSCs, perovskite solar cells; HTL, hole transporting layer.

The authors showed that the charge transport of the SnO_2 layer could be effectively improved by applying a after-treatment in the presence of water vapor. Apart from these metal oxides, Nb_2O_5 (Fig. 11(a)) [134], Zn_2SnO_4 [135], Al_2O_3 [136], and $W(Nb)O_X$ [137] have also been used as ETLs with high efficiencies of 18.4%, 15.3%, 14.6%, and 15.65%, respectively. It was found that Nb_2O_5 becomes an effective carrier extraction layer, which prohibits charge recombination, by the addition of dimethyl sulfide. To date, the best efficiency achieved for flexible PSCs is 18.4%.

3.2.1.1.2. Inverted p–i–n flexible PSCs. In this architecture, TCO is covered by a hole-transport material (HTM) compact layer, and the perovskite is coated by an ETL. For this structure, the material typically used as the HTM is PEDOT:PSS, a p-doped polymer, and the common ETL material deposited is phenyl-C61-butyric acid methyl ester (PCBM). These layers can be easily fabricated in solution, do not require high temperatures (<150 °C), and are thus compatible with polymer substrates. PSCs with a 6.4% efficiency were first reported based on a PET/ITO/PEDOT:PSS/perovskite/PCBM/TiO_2 sol-gel/Al structure, in which PEDOT:PSS performed well as a material for perovskite growth with good hole extracting capability [138]. To date, the highest efficiency of flexible PSC based on PEDOT:PSS is 17.3%, with a PEN/ITO/PEDOT:PSS/perovskite/C_{60}/BCP/LiF/Al architecture. However, this layer can become unstable in the presence of moisture. Therefore, encapsulation techniques as well as alternate materials should be developed for this layer. NiO_X and poly(triaryl amine) were also exploited as HTMs for flexible

PSCs (refer Fig. 11(b)), with the highest efficiencies achieved to date of 14.5% [139] and 18.1% [140], respectively. In the case of ETLs, PCBM showed higher charge extraction capability compared with TiO_2 [141]. When deposited on perovskite layers, PCBM can percolate through the grain boundaries, passivating the surface defects, thereby enhancing cell efficiency [142]. Most research on this architecture has focused on perovskite layers and further modification, especially on the implementation of the interlayer between interfaces. In the case of the perovskite/ETL interface, by adding NH_4Cl to the perovskite precursor solution, a smooth perovskite film was developed without thermal annealing, and a PCE of 9.32% was achieved [143]. In another report, $PbCl_2$ was mixed with perovskite in a precursor solution with a common ratio of 3:1 for CH_3NH_3I:$PbCl_2$, and the efficiency reached 14.5% [139]. In terms of the top interface, various materials have been used for further improvements, such as BIS-C60, LiF, ZnO, BCP, and TiO_2. Among them, the best efficiency of 18.1% was achieved with an architecture exploiting BCP.

3.2.1.2. TCO-free PEDOT:PSS. As mentioned previously, TCO is a brittle, high cost, and fragile material, and its applications in solar cells is limited because of which a substitute material that can be bent to a higher degree than regular electrodes is required [144]. At present, the typical material used to assume the role of the TCO is conductive PEDOT:PSS. Therefore, most TCO-free flexible PSCs are based on the inverted p−i−n architecture. The flexible device was fabricated on a 57-μm-thick polyethylene terephthalate based substrate, reaching a power conversion efficiency of 14% [145]. The highly efficient flexible PSCs were originated in its intrinsic optical and electrical properties as well as the well-made device architecture, which supports extracting charge carriers and high quality of perovskite layer. Further improvement of PEDOT:PSS conductivity using treatment at a high temperature of over 130 °C with methanesulfonic acid was investigated; however, the resulting efficiency was limited to 8% for flexible PSCs and 11% for rigid one PSCs [146]. The main enhancement was demonstrated to be due to the considerable conductivity and high transmittance of double-layer PEDOT:PSS. The work function of the employed electrode was increased from −5.0 to −4.8 V after acid treatment, which was convenient for charge-carrier transport to the PEDOT:PSS anode. This work demonstrated that acid-treated PEDOT:PSS transparent anodes can be an effective approach to develop highly efficient and mechanically flexible PV devices with PEDOT:PSS anode materials. An alternative to PEDOT:PSS was developed using the single-layer graphene on PEN, whose efficiency was reported to be 16.8% with no hysteresis (Fig. 10(c)) [147]. The high-efficiency perovskite-based flexible solar cells exhibited beading stability, and a PCE of over 90% of the original value within 1000 bending cycles was maintained. Transparent and ultrathin PET foils were used as substrates to achieve high power-per-weight PV devices as well as salient flexibility, and the foils exhibited a stabilized 12% efficiency over 5000 cycles and a high power-per-weight of 23 W/g [148]. The PEDOT:PSS conducting anode with a sheet resistance of 105 Ω/cm was prepared from Clevios PH1000 with 5 vol% dimethylsulphoxide and 0.5 vol% Zonyl FS-300 fluorosurfactant (fluka). A chromium oxide-chromium interlayer (Cr_2O_3/Cr) was used to shield the top contact metal for better device stability by reaction with oxidizing and halide-forming iodide material. The sheet resistance of PEDOT:PSS transparent electrodes was reduced from 85 to as low as 15 Ω/sp through solvent blend additives, after-treatments, and a mild oxygen plasma treatment, which resulted in an ITO-free PSCs efficiency of 10.5% [149].

3.2.1.2.1. Dielectric/metal/dielectric stacks. An attractive alternative to conventional TCOs is multilayered structural configuration dielectric/metal/dielectric (DMD) as a transparent conductor because of its low cost, excellent mechanical properties, and compatibility with large-scale fabrication at low temperature. The PSCs were first fabricated on an opaque cellulose paper substrate and exhibited a maximum power conversion efficiency of 2.7% using MoOx/Au/MoOx stacks as the hole extracting electrode [150]. Indium-free SnOx/Ag/SnOx multilayer transparent conducting electrodes were deposited onto a glass substrate which was fabricated by applying an 11 nm Ag layer by RF magnetron sputtering at room temperature [151]. The top transparent MoOx/Au/MoOx stacks had a favorable combination of transmittance up to 62.5% and sheet resistance as low as 9 Ω/square. A DMD transparent electrode composed of a MoO_3−Au−MoO_3 stack was fabricated by combining a top electrode with a thin layer (55 nm) perovskite with 13.6% efficiency [152]. In addition, DMD stacks were also investigated as transparent bottom electrodes for PSCs. A multilayer transparent electrode WO_3/Ag/WO_3 (WAW) was developed, and the effects of their contact angle and roughness behavior on the perovskite morphology and crystallization, as well as power conversion efficiency of PSCs were investigated [153]. The optimized morphology and crystal properties bring the maximum PCE of the flexible PSC based on the WAW transparent electrode is 8.04%, compared with the PCE of the controlled device is 10.51%. A SnOx/Ag/SnOx bottom electrode was developed by RF magnetron sputtering Ag, which was embedded on SnOx; a PCE of 11% was achieved. Optimized multilayered structures were tested as the bottom electrode for flexible PSCs with PET/SnO_2/Au/SnO_2 electrodes, and the electrodes showed a maximum PCE of 7.6% (V_{OC} = 0.923 V, J_{SC} = −14.09 mA/cm, FF = 58.29%), compared with a 5.4% PCE of PET/MoOx/Au/SnO_2 [154]. Ag was used as the metallic layer to prevent detrimental effects on the migration of Ag in the perovskite layer, which is known to make the device unstable. Therefore, the DMD electrode on the PET revealed remarkably stable electrical properties after bending at radius of as low as 1.5 mm.

3.2.1.2.2. Silver nanowires. AgNW networks are an attractive candidate for alternative TCO in PSCs due to their low sheet resistance, high transmittance, and solution processability [155]. Ag NWs were prepared by various synthesis methods such as ultraviolet light irradiation, polyol method, template method, and solvent thermal method. Ag NW network electrodes commonly achieved a sheet resistance of over 10 Ω/sq and transmittance of over 80% [156]. High quality and fully flexible Ag NWs were prepared between the monolayer graphene and mixed polymer matrix (polycarbonate:pc and additive) to develop flexible solar cells by the up-to-bottom method [157]. However, the halide in the liquid or vapor phase can easily penetrate the interfacial layer and can be absorbed on the AgNW surface. Therefore, the graphene layer and the polymer matrix were used as an inert layer to prevent oxidation and corrosion of the Ag mesh. Using the same approach, a flawless film composed of graphene oxide (GO) flakes was deposited on an AgNW network for preventing halide corrosion against AgNWs. A power conversion efficiency of 9.23% was achieved by controlling the amount of reduction reagents added to the GO precursor; this power conversion efficiency is suitable for the work function and surface wetting properties of the film [158]. The nanocomposite transparent electrode was deposited on a PET flexible substrate through a room temperature solution process to develop flexible PSCs; thus, this electrode could be prepared on a large-scale and at low temperatures. The hybrid AgNW/PEDOT:PSS electrode was slot-die coated using a roll-to-roll method and exhibited excellent transmittance and sheet resistance properties, which were similar to those of ITO which exhibited a champion efficiency of 11% [159]. A negligible change in efficiency appeared after 10,000 cycles after bending tests at a 5 mm radius. This paved the way for effective low-cost fabrication of truly flexible PSCs.

3.2.1.2.3. Graphene and CNTs. Carbon nanotubes and graphene can be applied as the BTE in both rigid and flexible PSCs because of their elemental constituent carbon and the mechanical resilience of carbon [160]. CNTs have high electrical conductivity and optical transparency, which enhance the performance of transparent carbon electrode-based devices. SWNT and graphene have been fabricated using flexible indium-free PSCs as the bottom flexible transparent electrode and their PV and mechanical properties have been investigated [161]. The carbon electrode-based PSC devices showed high reproducibility with no hysteresis and morphology, thus resulting in high efficiency. TCO-free PSCs were fabricated using SWNT by direct and dry-transferred method, and an efficiency of 6.32% was achieved [162]. A few nanometer-thick MoO_3 layers were added to enhance the wettability and work function of the graphene electrode to achieved a PCE of 17.1% on graphene-based PSCs, compared with 18.8% on ITO-based counterpart [163]. The low conductivity of the graphene electrode is compensated by the high transparency and the low surface roughness, resulting in a higher V_{OC} of the graphene device. We believe that the considerable potential of graphene and CNTs as a transparent electrode pave the way for a new paradigm of flexible PSCs and TCO-free devices.

3.2.1.3. Nanocellulose. To develop efficient solar cells, the following conditions must be fulfilled: high surface area and good charge transport properties for the PV effect so that photons can be effectively absorbed and converted into electricity. The performance and flexibility of solar cells need electrical, mechanical, and thermal properties and new materials are required than traditional electrical materials [164]. In the new challenges. Cellulose is a good candidate substrate for solar energy systems instead of thin glass, wafer, and metal foil. Cellulose can be easily produced from natural plants on earth. For various electronic applications, the nanoscale structures of cellulose's size, shape, and transparency are easily able to be controlled as similar to paper and microfibrillated cellulose (MFC) films, cellulose nanofibrils (CNF) films, and MFC-CNF composite films could be severed [165].

Gao et al. [166] developed PSCs fabricated on nanocellulose (NCP, ①-③ images in Fig. 10(a)). Nanocellulose (NC) viscous solution used to develop the substrate originated from natural cotton. A NC film exhibited good transparency of over 90% at a wavelength of 550 nm. The efficiencies of transparent bare acrylic resin and NCP/acrylic resin are 91.79% and 91.71% higher than that of common TCO films (ITO, AZO, IZO, and so on) (refer Fig. 10 (b)). Instead of FTO or ITO substrate, NC-based substrate can be used as a transparent substrate. PEDOT:PSS and aluminum were used as the anode and cathode electrode, respectively. Perovskite-related solutions were coated on the NCP substrate via spin-coating. Especially, PEDOT:PSS-coated NCP substrate has high transparency of over 90% and a sheet resistance of 14.4 kΩ/sq. The device structure of PSCs on the NCP-based substrate consisted of a doped PEDOT:PSS anode (40 nm)/PEDOT:PSS 4083 (30 nm)/perovskite (350 nm)/PCBM (100 nm)/Al (100 nm) (refer Fig. 10(c)). The best performance of the device was an efficiency of 4.25%, a V_{OC} of 0.69 V, a J_{SC} of 17.46 mA/cm, and a F.F. of 34.65% with a little gap between the forward and reverse modes (refer Fig. 10 (d)). As shown in Fig. 10(e), after bending 50 times via pushing the glass bottle of a diameter of 15 mm by hand, PCE values of the sample were varied under 10%. In addition, the performance of the NCP-based PSCs could be highly devolved with alternative materials (e.g. graphene, nanowires, nanotubes, nanosphere, and so on), advanced structures, and the devices fabrication process method [164,166,167].

3.2.2. Metal substrate

Metals are substitute materials for substrates when compared with their polymer counterparts. Compared with polymer substrates, they can withstand higher temperatures and exhibit a higher conductivity. The main issue when using metal foil is the requirement for manufacturing a transparent electrode on top of the perovskite layer without destroying it. For typical metal-based PSCs, mesoporous TiO_2 with an n–i–p architecture is used; therefore, in flexible PSCs, the metal substrate commonly exploited is Ti foil. The first results reported showed a PCE of 3.85% [168] which was obtained using a standard spray pyrolysis procedure to deposit a compact TiO_2 layer, followed by spin coating a mesoporous TiO_2 layer and a perovskite layer. Currently, the best PCE reported is 9.1% for Ti foil [169]. The top electrode consisted of Ag sputtered directly on top of the spiro layer, providing good conductivity and high transmittance. Further improvement using an Al_2O_3 scaffold layer was reported, and a PCE of 10.3% was observed with a Ti-foil/c-TiO_2/mp-Al_2O_3/perovskite/spiro/PEDOT:PSS/PET with an Ni mesh structure [170] (Fig. 11(d)).

In addition to nanoparticle-based structures, TiO_2 nanotubes or TiO_2 nanowalls have been used to fabricate flexible PSCs with efficiencies of 8.3% and 13.1%, respectively, which are the highest efficiencies reported in this field. Flexible PSCs have attracted significant attention because of their compatibility with R2R fabrication techniques. Moreover, they have the potential for practical application in portable, wearable, and lightweight electronic devices. Based on PSCs, which have several desirable qualities, including uniform morphology, highly crystalline structure orientation, and suitable bandgap, flexible PSCs can exhibit acceptable performance. Various methods have been developed to further improve flexible PSCs, such as modifying the synthesis technologies or tuning the proportions of the precursor. These methods have not only focused on the absorber layer but have also focused on the flexible interface, ETL, HTM, and electrode materials. Through concentrated efforts, the efficiency has increased to over 18% in the past few years. However, the limited flexibility and stability of flexible PSCs must be overcome for practical applications. Currently, the most reported flexible PSCs have a small area, similar to their glass substrate counterparts, because the PCE decreases significantly when upscaling from small-area to large-area cells. Therefore, effective upscaling techniques need to be developed for the fabrication of flexible PSCs.

3.3. Flexible colloidal quantum dot solar cells

Colloidal quantum dot solar cells (CQDSCs) have attracted considerable interest because of their size-tunable bandgap, solution processability, and high monodispersity [171–173]. The efficiencies of CQDSCs have rapidly improved to 12% using near-infrared (Eg = 1.3–1.4 eV) PbS nanocrystals [174]. CQDSCs have considerable potential for development of flexible or wearable electronic devices such as electronic textiles, artificial skins, and portable devices [57]. Zhang et al. [175] reported the use of transparent CNT films as an electrode layer in CQDSCs, which achieved a maximum PCE of 5.6% on a flexible substrate. Fig. 12(a) shows a schematic drawing of a CQDSC with a transparent SWCNT film as the front electrode. Fig. 12(b) illustrates a transparent SWCNT film, in which the light gray color indicates the substrate; the SEM image indicates that the film is uniformly deposited on the substrate. CQDSCs have been fabricated using several methods, such as spray coating, spin coating, or dip coating [176–179]. Among them, spray coating is compatible with R2R processing and can produce high-quality PV films that exhibit high PCEs [180,181]. Kramer et al. [182] explored the versatility of the spray-coating method in CQDSCs and achieved an average PCE of 6.7%. CQDSCs have been fabricated onto a spherical lens substrate with two axes of curvature, resulting in a device with a 5% PCE, confirming that the spraying method can be used on curved and flexible substrates. In

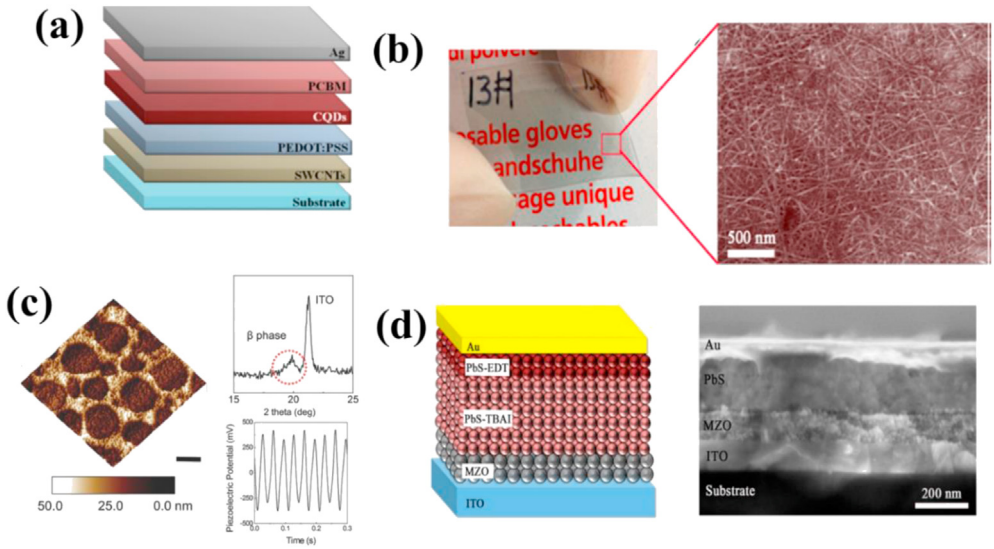

Fig. 12. (a) Schematic drawing of CQDSC with transparent SWCNT film and (b) photograph and SEM image of transparent SWCNT film press-transferred onto a flexible PET substrate. Reproduced with permission a study by Zhang et al. [175]. (c) Formation of β-phase P(VDF-TrFE) film after annealing, as measured by XRD. Reproduced with permission a study by Cho et al. [184]. (d) Schematic of device architecture and cross-sectional SEM image of fabricated CQDSC. Reproduced with permission from a study by Zhang et al. [185]. SWCNT, single-walled carbon nanotubes; CQDSCs, colloidal quantum dot solar cells; PET, polyethylene terephthalate.

other studies, the recombination pathway created during the fabrication process was damaged because of strain in the semiconducting layers, resulting in loss of charge carriers, which limited the performance of flexible QDSCs [183]. Therefore, to increase the performance of flexible QDSCs, boost yield, and reduce the recombination of photogenerated charges, the junction properties must be controlled. Cho et al. [184] added a porous piezoelectric poly(vinylidenefluoride-trifluoroethylene) (P(VDF-TrFE)) polymer layer between a ZnO ETL and a PbS QD heterojunction to modulate the junction properties and enhance the charge-carrier behavior at the QDSC junction. Fig. 12(c) illustrates the favorable piezoelectric effect, which formed a piezoelectric β-phase after applying a thermal annealing process. Thus, the current density was increased by 38%, and the PCE was increased by 37% because of the piezoelectric effect. Using a similar approach, Zhang reported a flexible CQD with improved electron extraction using MgZnO nanocrystals [185]. MgZnO (MZO) thin films with different Mg contents were used to decrease the interfacial recombination and enhance the solar cell efficiency. Fig. 12(d) shows a schematic diagram of the device architecture and a cross-sectional SEM image of the fabricated CQDSC. The solution-processed flexible PbS CQDSC fabricated using easily prepared MZO-NCs as the ETL at low temperature achieved a PCE of up to 9.4%, which is the highest value reported till date for flexible CQDSCs.

3.4. CIGS flexible solar cell

Until now, the PV market has been mainly dominated by silicon (Si)-based solar cells (92%) and cells based on cadmium telluride (CdTe, 5%), copper indium gallium selenide ($CuInGaSe_2$, CIGS < 2%), and amorphous silicon (a-Si:H, < 1%) [7,39,186]. In the future, the trend of the PV market will move to flexible electronics and related technologies. Considering the high efficiency, low-cost production, and production ability to develop many candidates of future PV technologies, CIGS is expected to be applied and used most quickly compared to other solar cells. CIGS is a second generation solar cell (thin-film type) and could be fabricated using non-vacuum and various vacuum-based techniques such as physical vapor deposition, pulsed laser deposition, metalorganic chemical vapor deposition (MOCVD), and sputtering. CIGS has been applied as a flexible solar cell, and the efficiency of CIGSS solar cells has been approaching 22.6% (approximately 25% expected by stimulation in Fig. 13(b)).

CIGS has been extensively studied for the substitution of silicon-based solar cells for a long time. Especially, as new materials such as different substrates (PI, metal foil, and cellulose) TCOs, and fabrications processes have been developed, CIGS has been rapidly used for developing flexible electronic applications. CIGS can be fabricated on various substrates such as silicon wafer, glass, metal foils, and polymers. Commercial CIGS on metal foils and polymers can be easily installed on any part of vehicles, on roofs of houses and buildings, and in portable electronics because they are lightweight and flexible and their sizes can be controlled. Even though they have various merits for application as flexible electronics, as shown in Fig. 13(c), CIGS has the disadvantage that its efficiency considerably depends on the type of substrate. As shown in Fig. 13(d), the cell efficiency has continued increase along with the theoretical efficiency. However, organic substrate to the inorganic substrate efficiency gap in cells is high. The choice of substrate is a very important consideration in terms of cell performance [186–189].

The cell efficiency of CIGS-based solar cells mainly affects the absorber band gap, doping concentration, and surface status (structure and morphology). CIGS is a ternary compound p-type semiconductor (I–III–VI_2 family) with tetragonal chalcopyrite $CuXY_2$ (X = In, Ga, Al, and Y =Se, S), and its structure is shown in Fig. 13(f). The crystal structure of CIGS consists of tetragonal distortion with Cu-Se, Ga-Se, or In-Se bonds. By tuning the bandgap of Cu, In, and Ga contents, not only the efficiency but also open-circuit voltage (V_{OC}) of cells can be improved. The bandgap can be tuned from 1.04 eV to 1.7 eV by controlling the ratio of each atom in triple complex Cu-In-Ga. Direct or indirect doping of CIGS is another appropriate alternative to enhance cell efficiency. Implanting impurities in the CIGS substrate can directly improve its efficiency; however, after CIGS cells are structurally formed, it would be difficult to confirm doping real effect inside CIGS via postdeposition treatment or evaporating at the designed gas atmosphere. During film growth, CIGS substrate can be implanted with alkali metals such as Li, Na, K, Rb, and Cs to improve the efficiency of cells compared to other attempts. Li and Na elements (light metal) are substituted in place of Cu sites, and Rb and Cs

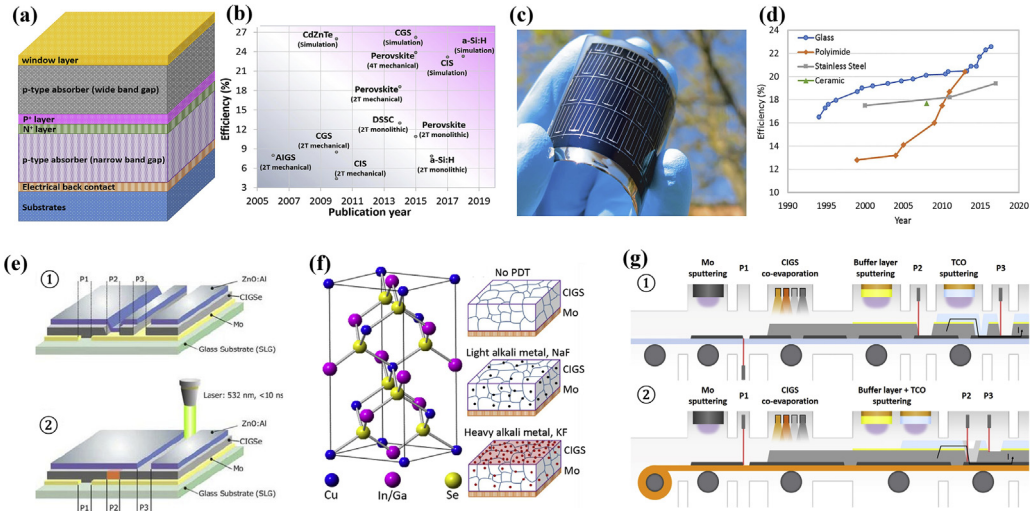

Fig. 13. (a) Basic multilayer structures of the CIGS thin-film-based solar cell. (b) Compassion of theoretical versus experimental cell efficiency. Reproduced with permission a study by Mufti et al. [187] (c) Photo of flexible CIGS device on polyimide with scribed individual cells (MgF2/i-ZnO/Al-ZnO/Cds/CIGS/Mo/glass substrate and (d) efficiency record of CIGS for various substrates. Reproduced with permission from Ramanujam et al. [188]. (e) The simplified scheme of monolithic interconnected CIGS modules on the rigid substrates with substrate-side P1 laser scribing① and polyimide substrates with single-aligned P2 and P3 laser scribing②, (f) crystal structure of CIGS and different roles of light and heavy alkali metal doping on the CIGS layer. Reproduced with permission a study by Stegemann et al. [189], and (g) Schematics of monolithically interconnected CIGS thin-film solar cell with P1, P2, and, P3 scribes to electrically isolate adjacent cells① and alternative approach for serial interconnection featuring a laser-transformed P2 trench②. Reproduced with permission a study by Wang et al. [190].

(heavy metal) contribute to the growth of secondary phases with Se and In. Zn is used to control the carrier concentration, wherein Zn can play the role of an acceptor to yield a ZnCu donor, which converts the CIGS film into an n-type layer. Furthermore, a p-type CIGS absorber layer can exhibit high carrier concentration by tuning the optimal composition of Zn in the three-stage deposition process. Finally, the development of the CIGS absorber layer is important because of its main contribution to light absorption. Another improvement in the efficiency is the enhanced surface morphology of the CIGS absorbance layer. This can approach two ways that are the deposition of n-type buffer layers on the CIGS layer and the smooth surface of the CIGS film as increasing light reflection from the film surface.

A recent Si-based solar cell module comprising monolithic cell-to-cell interconnections in series was developed by laser scribing without soldering a copper wire (ribbon) on the bus bar of the cell. CIGS thin films can be produced in the same Si-based solar cell production line if the substrate has some problems with the process. Fig. 13(e) and (g) shows the laser scribing process to develop cell-to-cell monolithic serial interconnections. The laser scribing process was performed in three steps: P1, P2, and P3. Between cells, P1 scribing creates narrow isolating trenches in the molybdenum (Mo) bottom substrates to dived into each cell. The P2 scribing removes the CIGS layers and exposes the Mo back to achieve current flow between adjacent cells with the connection usually made between TCO layers. The P3 scribing completes the cell separation by creating isolating trenches in the TCO layers. The distance between scribe lines and the width of scribe lines have to be minimized while avoiding the risk of short circuits due to the reduced dead area. The optimized laser scribing process can be adopted for CIGS with a flexible substrate such as PI, as shown in Fig. 13(g). Compared with conventional methods, monolithically interconnected layers developed via laser scribing can be used to develop affordable flexible solar cells; such cells have the advantage of a smaller dead area without degradation of cell performance [44–46,190].

4. Conclusions and outlook

In this review, we discuss the recent progress on flexible PV technologies from materials to the module systems. The important aspects to consider are the materials (metal and transparent electrodes), manufacturing methods, and combinations of interlayers to realize flexible PV devices. Beyond silicon-based PV technology, to dominate the PV market and wide to various applications, researchers should focus on three aspects: (1) efficiency and lifetime, (2) size scale-up, portability, and wearability, (3) cost-effectiveness and ecofriendliness. The efficiency of commercially used silicon-based solar cells is almost 25% (silicon-based tandem solar cells: near or above 30%). Silicon solar cells can be reliably employed for around 30 years regardless of the operation conditions such as moisture and oxygen levels and UV light. Compared with silicon-based solar cells, the recent flexible solar cells could satisfy the requirements of portability and wearability. However, the problems faced during increasing the size of cells and bending, such as loss of efficiency and stability, should be solved as soon as possible. Organic-based solar cells, especially PSCs, contain numerous harmful materials (such as Pb, Br, and Cl). Moreover, some materials (such as Spiro-OMeTAD) are much more expensive than other chemical materials. If the aforementioned problems are solved, flexible technologies could have a strong point to be enough covered not only in the conventional solar cell market but also flexible that in terms of cost and resources.

Declaration of competing interest

The authors declare that they have no known competing financial interests or personal relationships that could have appeared to influence the work reported in this paper.

Acknowledgments

This research was supported by Creative Materials Discovery Program through the National Research Foundation of Korea (NRF)

funded by the Ministry of Science and ICT (2017M3D1A1040828) and the grants from the National Research Foundation of Korea (NRF) funded by the Ministry of Science and ICT (NRF-2020R1F1A1076576) and by Korea Electric Power Corporation. (Grant Number: R18XA02).

References

[1] C. Guillen, J. Herrero, TCO/metal/TCO structures for energy and flexible electronics, Thin Solid Films 520 (1) (2011) 1–17.
[2] P.A. Owusu, S. Asumadu-Sarkodie, A review of renewable energy sources, sustainability issues and climate change mitigation, Cogent Eng. 3 (1) (2016), 1167990, 1-14.
[3] S.K. Ngoh, D. Njomo, An overview of hydrogen gas production from solar energy, Renew. Sustain. Energy Rev. 16 (9) (2012) 6782–6792.
[4] C. Jiang, S.J. Moniz, A. Wang, T. Zhang, J. Tang, Photoelectrochemical devices for solar water splitting–materials and challenges, Chem. Soc. Rev. 46 (15) (2017) 4645–4660.
[5] A. Luque, S. Hegedus, Handbook of Photovoltaic Science and Engineering, John Wiley & Sons, 2011.
[6] D. Lincot, The new paradigm of photovoltaics: from powering satellites to powering humanity, Compt. Rendus Phys. 18 (7–8) (2017) 381–390.
[7] F. Cardon, in: Photovoltaic and Photoelectrochemical Solar Energy Conversion, vol. 69, Springer Science & Business Media, 2012.
[8] D.E. Carlson, C.R. Wronski, Amorphous silicon cell, Appl. Phys. Lett. 28 (11) (1976) 671–673.
[9] B. Parida, S. Iniyan, R. Goic, A review of solar photovoltaic technologies, Renew. Sustain. Energy Rev. 15 (3) (2011) 1625–1636.
[10] K.A. Moharram, M. Abd-Elhady, H. Kandil, H. El-Sherif, Enhancing the performance of photovoltaic panels by water cooling, Ain Shams Eng. J. 4 (4) (2013) 869–877.
[11] A.A. Husain, W.Z.W. Hasan, S. Shafie, M.N. Hamidon, S.S. Pandey, A review of transparent solar photovoltaic technologies, Renew. Sustain. Energy Rev. 94 (2018) 779–791.
[12] K. Akhtar, N.A. Shad, M.M. Sajid, Y. Javed, M. Asif, K. Ali, H. Anwar, Y. Jamil, S. Sharma, Photovoltaic-based nanomaterials: synthesis and characterization, in: Solar Cells, Springer, 2020, pp. 139–158.
[13] G. Hashmi, K. Miettunen, T. Peltola, J. Halme, I. Asghar, K. Aitola, M. Toivola, P. Lund, Review of materials and manufacturing options for large area flexible dye solar cells, Renew. Sustain. Energy Rev. 15 (8) (2011) 3717–3732.
[14] Z. Li, T.R. Klein, D.H. Kim, M. Yang, J.J. Berry, M.F. van Hest, K. Zhu, Scalable fabrication of perovskite solar cells, Nat. Rev. Mater. 3 (4) (2018) 1–20.
[15] X. Xu, K. Fukuda, A. Karki, S. Park, H. Kimura, H. Jinno, N. Watanabe, S. Yamamoto, S. Shimomura, D. Kitazawa, Thermally stable, highly efficient, ultraflexible organic photovoltaics, Proc. Natl. Acad. Sci. Unit. States Am. 115 (18) (2018) 4589–4594.
[16] P. Yoon, H. Chung, H.-e. Song, J.H. Seo, S. Shin, Investigation of the controlling parameters on the bowing phenomenon in ultra-thin crystalline silicon solar cells, Appl. Therm. Eng. 90 (2015) 559–570.
[17] J.N. Burghartz, W. Appel, C. Harendt, H. Rempp, H. Richter, M. Zimmermann, Ultra-thin chip technology and applications, a new paradigm in silicon technology, Solid State Electron. 54 (9) (2010) 818–829.
[18] A. Blakers, T. Armour, Flexible silicon solar cells, Sol. Energy Mater. Sol. Cells 93 (8) (2009) 1440–1443.
[19] F. Brunetti, A. Operamolla, S. Castro-Hermosa, G. Lucarelli, V. Manca, G.M. Farinola, T.M. Brown, Printed solar cells and energy storage devices on paper substrates, Adv. Funct. Mater. 29 (21) (2019) 1806798.
[20] W.S. Koh, K.M. Lee, P.Y. Toh, S.P. Yeap, Nano-graphene and its derivatives for fabrication of flexible electronic devices: a quick review, Energy Convers. 40 (2018) 43.
[21] J.H. Lai, Polymers for Electronic Applications, CRC press, 2018.
[22] H. Cole, Properties of glass and plastics, Nature 167 (4241) (1951), 212-212.
[23] V. Zardetto, T.M. Brown, A. Reale, A. Di Carlo, Substrates for flexible electronics: a practical investigation on the electrical, film flexibility, optical, temperature, and solvent resistance properties, J. Polym. Sci. B Polym. Phys. 49 (9) (2011) 638–648.
[24] A. Gerthoffer, F. Roux, F. Emieux, P. Faucherand, H. Fournier, L. Grenet, S. Perraud, CIGS solar cells on flexible ultra-thin glass substrates: characterization and bending test, Thin Solid Films 592 (2015) 99–104.
[25] S. Sheehan, P. Surolia, O. Byrne, S. Garner, P. Cimo, X. Li, D. Dowling, K. Thampi, Flexible glass substrate based dye sensitized solar cells, Sol. Energy Mater. Sol. Cell. 132 (2015) 237–244.
[26] C. Yi, W. Li, S. Shi, K. He, P. Ma, M. Chen, C. Yang, High-temperature-resistant and colorless polyimide: preparations, properties, and applications, Sol. Energy 195 (2020) 340–354.
[27] J. Kim, S. Shrestha, M. Souri, J.G. Connell, S. Park, A. Seo, High-temperature optical properties of indium tin oxide thin-films, Sci. Rep. 10 (1) (2020) 1–8.
[28] Y.-N. Kim, H.-G. Shin, J.-K. Song, D.-H. Cho, H.-S. Lee, Y.-G. Jung, Thermal degradation behavior of indium tin oxide thin films deposited by radio frequency magnetron sputtering, J. Mater. Res. 20 (6) (2005) 1574–1579.
[29] S.J. Lee, Y. Kim, J.-Y. Hwang, J.-H. Lee, S. Jung, H. Park, S. Cho, S. Nahm, W.S. Yang, H. Kim, Flexible indium–tin oxide crystal on plastic substrates supported by graphene monolayer, Sci. Rep. 7 (1) (2017) 1–8.
[30] J.-I. Park, J.H. Heo, S.-H. Park, K.I. Hong, H.G. Jeong, S.H. Im, H.-K. Kim, Highly flexible InSnO electrodes on thin colourless polyimide substrate for high-performance flexible CH3NH3PbI3 perovskite solar cells, J. Power Sources 341 (2017) 340–347.
[31] U. Ali, K.J.B.A. Karim, N.A. Buang, A review of the properties and applications of poly (methyl methacrylate)(PMMA), Polym. Rev. 55 (4) (2015) 678–705.
[32] S. Sharma, S. Shriwastava, S. Kumar, K. Bhatt, C.C. Tripathi, Alternative transparent conducting electrode materials for flexible optoelectronic devices, Opto-Electron. Rev. 26 (3) (2018) 223–235.
[33] M.W. Rowell, M.D. McGehee, Transparent electrode requirements for thin film solar cell modules, Energy Environ. Sci. 4 (1) (2011) 131–134.
[34] S.D. Ponja, S. Sathasivam, I.P. Parkin, C.J. Carmalt, Highly conductive and transparent gallium doped zinc oxide thin films via chemical vapor deposition, Sci. Rep. 10 (1) (2020) 1–7.
[35] A. Alsaad, A. Ahmad, I. Qattan, Q.M. Al-Bataineh, Z. Albataineh, Structural, optoelectrical, linear, and nonlinear optical characterizations of dip-synthesized undoped ZnO and group III elements (B, Al, Ga, and In)-doped ZnO thin films, Crystals 10 (4) (2020) 252.
[36] D. Wang, Y. Zhang, X. Lu, Z. Ma, C. Xie, Z. Zheng, Chemical formation of soft metal electrodes for flexible and wearable electronics, Chem. Soc. Rev. 47 (12) (2018) 4611–4641.
[37] H. Ferhati, F. Djeffal, Performance assessment of TCO/metal/TCO multilayer transparent electrodes: from design concept to optimization, J. Comput. Electron. (2020) 1–10.
[38] M. Girtan, Comparison of ITO/metal/ITO and ZnO/metal/ZnO characteristics as transparent electrodes for third generation solar cells, Sol. Energy Mater. Sol. Cell. 100 (2012) 153–161.
[39] P. Ushasree, B. Bora, Silicon Solar Cells, 2019.
[40] Y. Hu, S. Ding, P. Chen, T. Seaby, J. Hou, L. Wang, Flexible solar-rechargeable energy system, Energy Storage Mater. 32 (2020) 356–376.
[41] M.T. Zarmai, N. Ekere, C. Oduoza, E.H. Amalu, A review of interconnection technologies for improved crystalline silicon solar cell photovoltaic module assembly, Appl. Energy 154 (2015) 173–182.
[42] V. Vega-Garita, L. Ramirez-Elizondo, N. Narayan, P. Bauer, Integrating a photovoltaic storage system in one device: a critical review, Prog. Photovoltaics Res. Appl. 27 (4) (2019) 346–370.
[43] M. Späth, P. Sommeling, J. Van Roosmalen, H. Smit, N. Van der Burg, D. Mahieu, N. Bakker, J. Kroon, Reproducible manufacturing of dye-sensitized solar cells on a semi-automated baseline, Prog. Photovoltaics Res. Appl. 11 (3) (2003) 207–220.
[44] L. Lucera, F. Machui, P. Kubis, H.-J. Egelhaaf, C.J. Brabec, In Highly efficient, large area, roll coated flexible and rigid solar modules: design rules and realization, in: 2016 IEEE 43rd Photovoltaic Specialists Conference (PVSC), IEEE, 2016, 0234-0237.
[45] A. Fakharuddin, R. Jose, T.M. Brown, F. Fabregat-Santiago, J. Bisquert, A perspective on the production of dye-sensitized solar modules, Energy Environ. Sci. 7 (12) (2014) 3952–3981.
[46] D.H. Kim, J.B. Whitaker, Z. Li, M.F. van Hest, K. Zhu, Outlook and challenges of perovskite solar cells toward terawatt-scale photovoltaic module technology, Joule 2 (8) (2018) 1437–1451.
[47] A.E. Ostfeld, A.M. Gaikwad, Y. Khan, A.C. Arias, High-performance flexible energy storage and harvesting system for wearable electronics, Sci. Rep. 6 (2016) 26122.
[48] T. Toyoda, T. Sano, J. Nakajima, S. Doi, S. Fukumoto, A. Ito, T. Tohyama, M. Yoshida, T. Kanagawa, T. Motohiro, Outdoor performance of large scale DSC modules, J. Photochem. Photobiol. Chem. 164 (1–3) (2004) 203–207.
[49] R. Sastrawan, J. Beier, U. Belledin, S. Hemming, A. Hinsch, R. Kern, C. Vetter, F. Petrat, A. Prodi-Schwab, P. Lechner, A glass frit-sealed dye solar cell module with integrated series connections, Sol. Energy Mater. Sol. Cell. 90 (11) (2006) 1680–1691.
[50] Y. Jun, J.-H. Son, D. Sohn, M.G. Kang, A module of a TiO2 nanocrystalline dye-sensitized solar cell with effective dimensions, J. Photochem. Photobiol. Chem. 200 (2–3) (2008) 314–317.
[51] E. Pascual-San-José, G. Sadoughi, L. Lucera, M. Stella, E. Martínez-Ferrero, G.E. Morse, M. Campoy-Quiles, I. Burgués-Ceballos, Towards photovoltaic windows: scalable fabrication of semitransparent modules based on non-fullerene acceptors via laser-patterning, J. Mater. Chem. 8 (19) (2020) 9882–9895.
[52] G.D. Spyropoulos, C.O.R. Quiroz, M. Salvador, Y. Hou, N. Gasparini, P. Schweizer, J. Adams, P. Kubis, N. Li, E. Spiecker, T. Ameri, H.-J. Egelhaaf, C.J. Brabec, Organic and perovskite solar modules innovated by adhesive top electrode and depth-resolved laser patterning, Energy Environ. Sci. 9 (7) (2016) 2302–2313.
[53] D.M. Chapin, C.S. Fuller, G.L. Pearson, A new silicon p-n junction photocell for converting solar radiation into electrical power, J. Appl. Phys. 25 (5) (1954) 676–677.
[54] S. Almosni, A. Delamarre, Z. Jehl, D. Suchet, L. Cojocaru, M. Giteau, B. Behaghel, A. Julian, C. Ibrahim, L. Tatry, H.B. Wang, T. Kubo, S. Uchida, H. Segawa, N. Miyashita, R. Tamaki, Y. Shoji, K. Yoshida, N. Ahsan, K. Watanabe, T. Inoue, M. Sugiyama, Y. Nakano, T. Hamamura, T. Toupance, C. Olivier, S. Chambon, L. Vignau, C. Geffroy, E. Cloutet, G. Hadziioannou, N. Cavassilas, P. Rale, A. Cattoni, S. Collin, F. Gibelli, M. Paire, L. Lombez,

D. Aureau, M. Bouttemy, A. Etcheberry, Y. Okada, J.F. Guillemoles, Material challenges for solar cells in the twenty-first century: directions in emerging technologies, Sci. Technol. Adv. Mater. 19 (1) (2018) 336–369.
[55] L.C. Andreani, A. Bozzola, P. Kowalczewski, M. Liscidini, L. Redorici, Silicon solar cells: toward the efficiency limits, Adv. Phys.X 4 (1) (2019) 1–25.
[56] Y.Y. Liang, Z. Xu, J.B. Xia, S.T. Tsai, Y. Wu, G. Li, C. Ray, L.P. Yu, For the bright future-bulk heterojunction polymer solar cells with power conversion efficiency of 7.4%, Adv. Mater. 22 (20) (2010) E135–E138.
[57] M. Kaltenbrunner, M.S. White, E.D. Glowacki, T. Sekitani, T. Someya, N.S. Sariciftci, S. Bauer, Ultrathin and lightweight organic solar cells with high flexibility, Nat. Commun. 3 (770) (2012) 1–7.
[58] Q. Burlingame, C. Coburn, X.Z. Che, A. Panda, Y. Qu, S.R. Forrest, Centimetre-scale electron diffusion in photoactive organic heterostructures, Nature 554 (7690) (2018) 77–80.
[59] Y.B. Lin, Y.Z. Jin, S. Dong, W.H. Zheng, J.Y. Yang, A.L. Liu, F. Liu, Y.F. Jiang, T.P. Russell, F.L. Zhang, F. Huang, L.T. Hou, Printed nonfullerene organic solar cells with the highest efficiency of 9.5%, Adv. Energy Mater. 8 (1701942) (2018) 1–8.
[60] P. Cheng, G. Li, X.W. Zhan, Y. Yang, Next-generation organic photovoltaics based on non-fullerene acceptors, Nat. Photonics 12 (3) (2018) 131–142.
[61] L. Mao, J.H. Tong, S.X. Xiong, F.Y. Jiang, F. Qin, W. Meng, B.W. Luo, Y. Liu, Z.F. Li, Y.Y. Jiang, C. Fuentes-Hernandez, B. Kippelen, Y.H. Zhou, Flexible large-area organic tandem solar cells with high defect tolerance and device yield, J. Mater. Chem. A 5 (7) (2017) 3186–3192.
[62] Y. Zhang, H.F. Yao, S.Q. Zhang, Y.P. Qin, J.Q. Zhang, L.Y. Yang, W.N. Li, Z.X. Wei, F. Gao, J.H. Hou, Fluorination vs. chlorination: a case study on high performance organic photovoltaic materials, Sci. China Chem. 61 (10) (2018) 1328–1337.
[63] L.X. Meng, Y.M. Zhang, X.J. Wan, C.X. Li, X. Zhang, Y.B. Wang, X. Ke, Z. Xiao, L.M. Ding, R.X. Xia, H.L. Yip, Y. Cao, Y.S. Chen, Organic and solution-processed tandem solar cells with 17.3% efficiency, Science 361 (6407) (2018) 1094–1098.
[64] H. Li, Z. Xiao, L.M. Ding, J.Z. Wang, Thermostable single-junction organic solar cells with a power conversion efficiency of 14.62%, Sci. Bull. 63 (6) (2018) 340–342.
[65] W. Song, X. Fan, B.G. Xu, F. Yan, H.Q. Cui, Q. Wei, R.X. Peng, L. Hong, J.M. Huang, Z.Y. Ge, All-solution-processed metal-oxide-free flexible organic solar cells with over 10% efficiency, Adv. Mater. 30 (180075) (2018) 1–8.
[66] S.X. Xiong, L. Hu, L. Hu, L.L. Sun, F. Qin, X.J. Liu, M. Fahlman, Y.H. Zhou, 12.5% Flexible nonfullerene solar cells by passivating the chemical interaction between the active layer and polymer interfacial layer, Adv. Mater. 31 (1806616) (2019) 1–7.
[67] Y.X. Zhang, J. Fang, W. Li, Y. Shen, J.D. Chen, Y.Q. Li, H.W. Gu, S. Pelivani, M.J. Zhang, Y.F. Li, J.X. Tang, Synergetic transparent electrode architecture for efficient non-fullerene flexible organic solar cells with > 12% efficiency, ACS Nano 13 (4) (2019) 4686–4694.
[68] D.S. Hecht, L.B. Hu, G. Irvin, Emerging transparent electrodes based on thin films of carbon nanotubes, graphene, and metallic nanostructures, Adv. Mater. 23 (13) (2011) 1482–1513.
[69] S.P. Pang, Y. Hernandez, X.L. Feng, K. Mullen, Sraphene as transparent electrode material for organic electronics, Adv. Mater. 23 (25) (2011) 2779–2795.
[70] T.H. Han, Y. Lee, M.R. Choi, S.H. Woo, S.H. Bae, B.H. Hong, J.H. Ahn, T.W. Lee, Extremely efficient flexible organic light-emitting diodes with modified graphene anode, Nat. Photonics 6 (2) (2012) 105–110.
[71] R.Y. Liu, M.L. Tan, X.H. Zhang, L. Xu, J.J. Chen, Y. Chen, X.Y. Tang, L.M. Wan, Solution-processed composite electrodes composed of silver nanowires and aluminum-doped zinc oxide nanoparticles for thin-film solar cells applications, Sol. Energy Mater Sol. Cells 174 (2018) 584–592.
[72] J.Y. Lee, S.T. Connor, Y. Cui, P. Peumans, Solution-processed metal nanowire mesh transparent electrodes, Nano Lett. 8 (2) (2008) 689–692.
[73] J.Y. Zou, C.Z. Li, C.Y. Chang, H.L. Yip, A.K.Y. Jen, Interfacial engineering of ultrathin metal film transparent electrode for flexible organic photovoltaic cells, Adv. Mater. 26 (22) (2014) 3618–3623.
[74] B.W. An, B.G. Hyun, S.Y. Kim, M. Kim, M.S. Lee, K. Lee, J.B. Koo, H.Y. Chu, B.S. Bae, J.U. Park, Stretchable and transparent electrodes using hybrid structures of graphene-metal nanotrough networks with high performances and ultimate uniformity, Nano Lett. 14 (11) (2014) 6322–6328.
[75] M. Reidinger, M. Rydzek, C. Scherdel, M. Arduini-Schuster, J. Manara, Low-emitting transparent coatings based on tin doped indiumoxide applied via a sol-gel routine, Thin Solid Films 517 (10) (2009) 3096–3099.
[76] I. Hamberg, C.G. Granqvist, Evaporated Sn-doped In2O3films: Basic optical properties and applications to energy-efficient windows, J. Appl. Phys. 60 (11) (1986) R123–R160.
[77] A. Tuna, Y. Selamet, G. Aygun, L. Ozyuzer, High quality ITO thin films grown by dc and RF sputtering without oxygen, J. Phys. D Appl. Phys. 43 (5) (2010).
[78] C.L. Kim, C.W. Jung, Y.J. Oh, D.E. Kim, A highly flexible transparent conductive electrode based on nanomaterials, NPG Asia Mater. 9 (2017) e438-e438.
[79] S.K. Hau, H.L. Yip, N.S. Baek, J.Y. Zou, K. O'Malley, A.K.Y. Jen, Air-stable inverted flexible polymer solar cells using zinc oxide nanoparticles as an electron selective layer, Appl. Phys. Lett. 92 (25) (2008), 2553301/1-3.
[80] I.C. Wang, W.T. Weng, M.Y. Tsai, M.K. Lee, S.F. Horng, T.P. Perng, C.C. Kei, C.C. Yu, H.F. Meng, Highly efficient flexible inverted organic solar cells using atomic layer deposited ZnO as electron selective layer, J. Mater. Chem. 20 (5) (2010) 862–866.
[81] C.Y. Chang, Y.J. Cheng, S.H. Hung, J.S. Wu, W.S. Kao, C.H. Lee, C.S. Hsu, Combination of molecular, morphological, and interfacial engineering to achieve highly efficient and stable plastic solar cells, Adv. Mater. 24 (4) (2012) 549–553.
[82] W.J. da Silva, H.P. Kim, A.R.B. Yusoff, J. Jang, Transparent flexible organic solar cells with 6.87% efficiency manufactured by an all-solution process, Nanoscale 5 (19) (2013) 9324–9329.
[83] B.F. Zhao, Z.C. He, X.P. Cheng, D.H. Qin, M. Yun, M.J. Wang, X.D. Huang, J.G. Wu, H.B. Wu, Y. Cao, Flexible polymer solar cells with power conversion efficiency of 8.7%, J. Mater. Chem. C 2 (26) (2014) 5077–5082.
[84] Y.W. Li, G.Y. Xu, C.H. Cui, Y.F. Li, Flexible and semitransparent organic solar cells, Adv. Energy Mater. 8 (7) (2018).
[85] I. Kim, S.H. Bae, C.T. Toh, H. Kim, J.H. Cho, D. Whang, T.W. Lee, B. Ozyilmaz, J.H. Ahn, Ultrathin organic solar cells with graphene doped by ferroelectric polarization, ACS Appl. Mater. Interfaces 6 (5) (2014) 3299–3304.
[86] F. Bonaccorso, Z. Sun, T. Hasan, A.C. Ferrari, Graphene photonics and optoelectronics, Nat. Photonics 4 (9) (2010) 611–622.
[87] H. Park, S. Chang, M. Smith, S. Gradecak, J. Kong, Interface engineering of graphene for universal applications as both anode and cathode in organic photovoltaics, Sci. Rep. 3 (1581) (2013) 1–18.
[88] Y. Wang, X.H. Chen, Y.L. Zhong, F.R. Zhu, K.P. Loh, Large area, continuous, few-layered graphene as anodes in organic photovoltaic devices, Appl. Phys. Lett. 95 (6) (2009), 063302/1-3.
[89] H. Park, P.R. Brown, V. Buloyic, J. Kong, Graphene as transparent conducting electrodes in organic photovoltaics: studies in graphene morphology, hole transporting layers, and counter electrodes, Nano Lett. 12 (1) (2012) 133–140.
[90] H. Park, J.A. Rowehl, K.K. Kim, V. Bulovic, J. Kong, Doped graphene electrodes for organic solar cells, Nanotechnology 21 (50) (2010).
[91] Z.Y. Zhao, J.D. Fite, P. Haldar, J.U. Lee, Enhanced ultraviolet response using graphene electrodes in organic solar cells, Appl. Phys. Lett. 101 (6) (2012), https://doi.org/10.1063/1.4742928.
[92] I.S. Shin, H. Jo, H.J. Shin, W.M. Choi, J.Y. Choi, S.W. Kim, High quality graphene-semiconducting oxide heterostructure for inverted organic photovoltaics, J. Mater. Chem. 22 (26) (2012) 13032–13038.
[93] Z.Y. Yin, S.Y. Sun, T. Salim, S.X. Wu, X.A. Huang, Q.Y. He, Y.M. Lam, H. Zhang, Organic photovoltaic devices using highly flexible reduced graphene oxide films as transparent electrodes, ACS Nano 4 (9) (2010) 5263–5268.
[94] D. Konios, C. Petridis, G. Kakavelakis, M. Sygletou, K. Savva, E. Stratakis, E. Kymakis, Reduced graphene oxide micromesh electrodes for large area, flexible, organic photovoltaic devices, Adv. Funct. Mater. 25 (15) (2015) 2213–2221.
[95] X.S. Li, W.W. Cai, J.H. An, S. Kim, J. Nah, D.X. Yang, R. Piner, A. Velamakanni, I. Jung, E. Tutuc, S.K. Banerjee, L. Colombo, R.S. Ruoff, Large-area synthesis of high-quality and uniform graphene films on copper foils, Science 324 (5932) (2009) 1312–1314.
[96] Z.K. Liu, J.H. Li, F. Yan, Package-free flexible organic solar cells with graphene top electrodes, Adv. Mater. 25 (31) (2013) 4296–4301.
[97] A.R.B. Yusoff, D. Kim, F.K. Schneider, W.J. da Silva, J. Jang, Au-doped single layer graphene nanoribbons for a record-high efficiency ITO-free tandem polymer solar cell, Energy Environ. Sci. 8 (5) (2015) 1523–1537.
[98] D.H. Zhang, K. Ryu, X.L. Liu, E. Polikarpov, J. Ly, M.E. Tompson, C.W. Zhou, Transparent, conductive, and flexible carbon nanotube films and their application in organic light-emitting diodes, Nano Lett. 6 (9) (2006) 1880–1886.
[99] J. Li, L. Hu, L. Wang, Y. Zhou, G. Gruner, T.J. Marks, Organic light-emitting diodes having carbon nanotube anodes, Nano Lett. 6 (11) (2006) 2472–2477.
[100] I.W. Rowell, M.A. Topinka, M.D. McGehee, H.J. Prall, G. Dennler, N.S. Sariciftci, L.B. Hu, G. Gruner, Organic solar cells with carbon nanotube network electrodes, Appl. Phys. Lett. 88 (23) (2006).
[101] A.G. Nasibulin, A. Kaskela, K. Mustonen, A.S. Anisimov, V. Ruiz, S. Kivisto, S. Rackauskas, M.Y. Timmermans, M. Pudas, B. Aitchison, M. Kauppinen, D.P. Brown, O.G. Okhotnikov, E.I. Kauppinen, Multifunctional free-standing single-walled carbon nanotube films, ACS Nano 5 (4) (2011) 3214–3221.
[102] I. Jeon, K. Cui, T. Chiba, A. Anisimov, A.G. Nasibulin, E.I. Kauppinen, S. Maruyama, Y. Matsuo, Direct and dry deposited single-walled carbon nanotube films doped with moox as electron-blocking transparent electrodes for flexible organic solar cells, J. Am. Chem. Soc. 137 (25) (2015) 7982–7985, rkskek.
[103] F.L. Zhang, M. Johansson, M.R. Andersson, J.C. Hummelen, O. Inganas, Polymer photovoltaic cells with conducting polymer anodes, Adv. Mater. 14 (9) (2002) 662–665.
[104] W. Meng, R. Ge, Z.F. Li, J.H. Tong, T.F. Liu, Q. Zhao, S.X. Xiong, F.Y. Jiang, L. Mao, Y.H. Zhou, Conductivity enhancement of PEDOT:PSS films via phosphoric acid treatment for flexible all-plastic solar cells, ACS Appl. Mater. Interfaces 7 (25) (2015) 14089–14094.
[105] Y.J. Xia, J.Y. Ouyang, PEDOT:PSS films with significantly enhanced conductivities induce Record efficiency stable d by preferential solvation with cosolvents and their application in polymer photovoltaic cells, J. Mater. Chem. 21 (13) (2011) 4927–4936.
[106] X. Fan, B.G. Xu, S.H. Liu, C.H. Cui, J.Z. Wang, F. Yan, Transfer-printed PEDOT:PSS electrodes using mild acids for high conductivity and improved stability with application to flexible organic solar cells, ACS Appl. Mater. Interfaces 8 (22) (2016) 14029–14036.

[107] Z.B. Yu, Q.W. Zhang, L. Li, Q. Chen, X.F. Niu, J. Liu, Q.B. Pei, Highly flexible silver nanowire electrodes for shape-memory polymer light-emitting diodes, Adv. Mater. 23 (5) (2011) 664–668.
[108] S. De, T.M. Higgins, P.E. Lyons, E.M. Doherty, P.N. Nirmalraj, W.J. Blau, J.J. Boland, J.N. Coleman, Silver nanowire networks as flexible, transparent, conducting films: extremely high DC to optical conductivity ratios, ACS Nano 3 (7) (2009) 1767–1774.
[109] I.W. Lim, D.Y. Cho, Jihoon-Kim, S.I. Na, H.K. Kim, Simple brush-painting of flexible and transparent Ag nanowire network electrodes as an alternative ITO anode for cost-efficient flexible organic solar cells, Sol. Energy Mater Sol. Cells 107 (2012) 348–354.
[110] I. Song, D.S. You, K. Lim, S. Park, S. Jung, C.S. Kim, D.H. Kim, D.G. Kim, J.K. Kim, J. Park, Y.C. Kang, J. Heo, S.H. Jin, J.H. Park, J.W. Kang, Highly efficient and bendable organic solar cells with solution-processed silver nanowire electrodes, Adv. Funct. Mater. 23 (34) (2013) 4177–4184.
[111] H. Seo, H.D. Um, A. Shukla, I. Hwang, J. Park, Y.C. Kang, C.S. Kim, M. Song, K. Seo, Low-temperature solution-processed flexible organic solar cells with PFN/AgNWs cathode, Nano Energy 16 (2015) 122–129.
[112] J.H. Seo, I. Hwang, H.D. Um, S. Lee, K. Lee, J. Park, H. Shin, T.H. Kwon, S.J. Kang, K. Seo, Cold isostatic-pressured silver nanowire electrodes for flexible organic solar cells via room-temperature processes, Adv. Mater. 29 (30) (2017).
[113] T. Lei, R.X. Peng, W. Song, L. Hong, J.M. Huang, N.N. Fei, Z.Y. Ge, Bendable and foldable flexible organic solar cells based on Ag nanowire films with 10.30% efficiency, J. Mater. Chem. A 7 (8) (2019) 3737–3744.
[114] X.Y. Dong, P. Shi, L.L. Sun, J. Li, F. Qin, S.X. Xiong, T.F. Liu, X.S. Jiang, Y.H. Zhou, Flexible nonfullerene organic solar cells based on embedded silver nanowires with an efficiency up to 11.6%, J. Mater. Chem. A 7 (5) (2019) 1989–1995.
[115] K.M. Rabe, M. Dawber, C. Lichtensteiger, C.H. Ahn, J.-M. Triscone, Moderns physics of ferroelectrics: essential background, in: Physics of Ferroelectrics: A Modern Perspective, 2007, pp. 1–30.
[116] F. Di Giacomo, A. Fakharuddin, R. Jose, T.M. Brown, Progress, challenges and perspectives in flexible perovskite solar cells, Energy Environ. Sci. 9 (10) (2016) 3007–3035.
[117] T. Gebauer, G. Schmid, Inorganic-organic hybrid structured LED's, Z. Anorg. Allg. Chem. 625 (7) (1999) 1124–1128.
[118] D.B. Mitzi, C.D. Dimitrakopoulos, L.L. Kosbar, Structurally tailored organic-inorganic perovskites: optical properties and solution-processed channel materials for thin-film transistors, Chem. Mater. 13 (10) (2001) 3728–3740.
[119] A. Kojima, K. Teshima, Y. Shirai, T. Miyasaka, Organometal halide perovskites as visible-light sensitizers for photovoltaic cells, J. Am. Chem. Soc. 131 (17) (2009) 6050–6051.
[120] I.P. Boix, K. Nonomura, N. Mathews, S.G. Mhaisalkar, Current progress and future perspectives for organic/inorganic perovskite solar cells, Mater. Today 17 (1) (2014) 16–23.
[121] I.F. Dong, Y.J. Fang, Y.C. Shao, P. Mulligan, J. Qiu, L. Cao, J.S. Huang, Electron-hole diffusion lengths > 175 mu m in solution-grown $CH_3NH_3PbI_3$ single crystals, Science 347 (6225) (2015) 967–970.
[122] Chart NREL Efficiency Chart, 2017. https://www.nrel.gov/pv/cell-efficiency.html.
[123] F. Qiao, L. Lu, P. Han, D. Ge, Y. Rui, D. Gu, T. Zhang, J. Hou, Y. Yang, A combined experimental and theoretical Study of Screen-printing High transparent conductive Mesoscopic ito films, Sci. Rep. 10 (1) (2020) 1–11.
[124] Y. Dkhissi, F.Z. Huang, S. Rubanov, M.D. Xiao, U. Bach, L. Spiccia, R.A. Caruso, Y.B. Cheng, Low temperature processing of flexible planar perovskite solar cells with efficiency over 10%, J. Power Sources 278 (2015) 325–331.
[125] C. Roldan-Carmona, O. Malinkiewicz, A. Soriano, G.M. Espallargas, A. Garcia, P. Reinecke, T. Kroyer, M.I. Dar, M.K. Nazeeruddin, H.J. Bolink, Flexible high efficiency perovskite solar cells, Energy Environ. Sci. 7 (3) (2014) 994–997.
[126] I. Wali, A. Fakharuddin, I. Ahmed, M.H. Ab Rahim, J. Ismail, R. Jose, Multi-porous nanofibers of SnO2 by electrospinning for high efficiency dye-sensitized solar cells, J. Mater. Chem. A 2 (41) (2014) 17427–17434.
[127] I. Wali, A. Fakharuddin, A. Yasin, M.H. Ab Rahim, J. Ismail, R. Jose, One pot synthesis of multi-functional tin oxide nanostructures for high efficiency dye-sensitized solar cells, J. Alloys Compd. 646 (2015) 32–39.
[128] Q. Wali, A. Fakharuddin, R. Jose, Tin oxide as a photoanode for dye-sensitised solar cells: current progress and future challenges, J. Power Sources 293 (2015) 1039–1052.
[129] I.H. Kumar, N. Yantara, S. Dharani, M. Graetzel, S. Mhaisalkar, P.P. Boix, N. Mathews, Flexible, low-temperature, solution processed ZnO-based perovskite solid state solar cells, Chem. Commun. 49 (94) (2013) 11089–11091.
[130] J.H. Heo, M.H. Lee, H.J. Han, B.R. Patil, J.S. Yu, S.H. Im, Highly efficient low temperature solution processable planar type CH3NH3PbI3 perovskite flexible solar cells, J. Mater. Chem. A 4 (5) (2016) 1572–1578.
[131] X. Dong, H.W. Hu, B.C. Lin, J.N. Ding, N.Y. Yuan, The effect of ALD-Zno layers on the formation of $CH_3NH_3PbI_3$ with different perovskite precursors and sintering temperatures, Chem. Commun. 50 (92) (2014) 14405–14408.
[132] I.S. Mali, C.K. Hong, A.I. Inamdar, H. Im, S.E. Shim, Efficient planar n-i-p type heterojunction flexible perovskite solar cells with sputtered TiO_2 electron transporting layers, Nanoscale 9 (9) (2017) 3095–3104.
[133] C.L. Wang, L. Guan, D.W. Zhao, Y. Yu, C.R. Grice, Z.N. Song, R.A. Awni, J. Chen, J.B. Wang, X.Z. Zhao, Y.F. Yan, Water vapor treatment of low-temperature deposited SnO_2 electron selective layers for efficient flexible perovskite solar cells, ACS Energy Lett. 2 (9) (2017) 2118–2124.
[134] J.S. Feng, X.J. Zhu, Z. Yang, X.R. Zhang, J.Z. Niu, Z.Y. Wang, S.N. Zuo, S. Priya, S.Z. Liu, D. Yang, Record efficiency stable flexible perovskite solar cell using effective additive assistant strategy, Adv. Mater. 30 (35) (2018).
[135] I.S. Shin, W.S. Yang, J.H. Noh, J.H. Suk, N.J. Jeon, J.H. Park, J.S. Kim, W.M. Seong, S.I. Seok, High-performance flexible perovskite solar cells exploiting Zn_2SnO_4 prepared in solution below 100 degrees C, Nat. Commun. 6 (2015) 1–8.
[136] J. Wei, H. Li, Y.C. Zhao, W.K. Zhou, R. Fu, H.Y. Pan, Q. Zhao, Flexible perovskite solar cells based on the metal-insulator-semiconductor structure, Chem. Commun. 52 (71) (2016) 10791–10794.
[137] K. Wang, Y.T. Shi, L.G. Gao, R.H. Chi, K. Shi, B.Y. Guo, L. Zhao, T.L. Ma, W.(Nb, O_X-based efficient flexible perovskite solar cells: from material optimization to working principle, Nano Energy 31 (2017) 424–431.
[138] P. Docampo, J.M. Ball, M. Darwich, G.E. Eperon, H.J. Snaith, Efficient organometal trihalide perovskite planar-heterojunction solar cells on flexible polymer substrates, Nat. Commun. 4 (1) (2013) 1–6.
[139] H. Zhang, J.Q. Cheng, F. Lin, H.X. He, J. Mao, K.S. Wong, A.K.Y. Jen, W.C.H. Choy, Pinhole-free and surface-nanostructured NiOx film by room-temperature solution process for high-performance flexible perovskite solar cells with good stability and reproducibility, ACS Nano 10 (1) (2016) 1503–1511.
[140] C. Bi, B. Chen, H.T. Wei, S. DeLuca, J.S. Huang, Efficient flexible solar cell based on composition-tailored hybrid perovskite, Adv. Mater. 29 (16505900) (2017) 1–6.
[141] K. Wojciechowski, T. Leijtens, S. Siprova, C. Schlueter, M.T. Horantner, J.T.W. Wang, C.Z. Li, A.K.Y. Jen, T.L. Lee, H.J. Snaith, C-60 as an efficient n-type compact layer in perovskite solar cells, J. Phys. Chem. Lett. 6 (12) (2015) 2399–2405.
[142] Y.H. Shao, Z.G. Xiao, C. Bi, Y.B. Yuan, J.S. Huang, Origin and elimination of photocurrent hysteresis by fullerene passivation in CH3NH3PbI3 planar heterojunction solar cells, Nat. Commun. 5 (5784) (2014) 1–7.
[143] Y.N. Chen, Y.X. Zhao, Z.Q. Liang, Non-thermal annealing fabrication of efficient planar perovskite solar cells with inclusion of NH4Cl, Chem. Mater. 27 (5) (2015) 1448–1451.
[144] I. Dianetti, F. Di Giacomo, G. Polino, C. Ciceroni, A. Liscio, A. D'Epifanio, S. Licoccia, T.M. Brown, A. Di Carlo, F. Brunetti, TCO-free flexible organo metal trihalide perovskite planar-heterojunction solar cells, Sol. Energy Mater Sol. Cells 140 (2015) 150–157.
[145] Y. Xia, K. Sun, J. Quyang, Solution-processed metallic conducting polymer films as transparent electrode of optoelectronic devices, Adv. Mater. 24 (18) (2012) 2436–2440.
[146] K. Sun, P.C. Li, Y.J. Xia, J.J. Chang, J.Y. Ouyang, Transparent conductive oxide-free perovskite solar cells with PEDOT:PSS as transparent electrode, ACS Appl. Mater. Interfaces 7 (28) (2015) 15314–15320.
[147] J. Yoon, H. Sung, G. Lee, W. Cho, N. Ahn, H.S. Jung, M. Choi, Superflexible, high-efficiency perovskite solar cells utilizing graphene electrodes: towards future foldable power sources, Energy Environ. Sci. 10 (1) (2017) 337–345.
[148] D. Liu, T.L. Kelly, Fatigue resistance of a flexible, efficient, and metal oxide-free perovskite solar cell, J. Mater. Chem. 3 (17) (2015) 9241–9248.
[149] B. Vaagensmith, K.M. Reza, M. Hasan, H. Elbohy, N. Adhikari, A. Dubey, N. Kantack, E. Gaml, Q.Q. Qiao, Environmentally friendly plasma-treated PEDOT:PSS as electrodes for ito-free perovskite solar cells, ACS Appl. Mater. Interfaces 9 (2017) 35861–35870.
[150] S. Castro-Hermosa, J. Dagar, A. Marsella, T.M. Brown, Perovskite solar cells on paper and the role of substrates and electrodes on performance, IEEE Electron. Device Lett. 38 (9) (2017) 1278–1281.
[151] J.-D. Yang, S.-H. Cho, T.-W. Hong, D.I. Son, D.-H. Park, K.-H. Yoo, W.-K. Choi, Organic photovoltaic cells fabricated on a SnOx/Ag/SnOx multilayer transparent conducting electrode, Thin Solid Films 520 (19) (2012) 6215–6220.
[152] E. Della Gaspera, Y. Peng, Q. Hou, L. Spiccia, U. Bach, J.J. Jasieniak, Y.-B. Cheng, Ultra-thin high efficiency semitransparent perovskite solar cells, Nano Energy 13 (2015) 249–257.
[153] X. Liu, X. Guo, Z. Gan, N. Zhang, X. Liu, Efficient perovskite solar cells based on multilayer transparent electrodes through morphology control, J. Phys. Chem. C 120 (47) (2016) 26703–26709.
[154] G. Lucarelli, T.M. Brown, Development of highly bendable transparent window electrodes based on MoOx, SnO_2, and Au dielectric/metal/dielectric stacks: application to indium tin Oxide (ITO)-free perovskite solar cells, Front. Mater. 6 (310) (2019) 1–11.
[155] C.H. Chung, T.B. Song, B. Bob, R. Zhu, H.S. Duan, Y. Yang, Silver nanowire composite window layers for fully solution-deposited thin-film photovoltaic devices, Adv. Mater. 24 (40) (2012) 5499–5504.
[156] J. Jiu, K. Suganuma, Metallic nanowires and their application, IEEE Trans. Compon. Packag. Manuf. Technol. 6 (12) (2016) 1733–1751.
[157] H. Dong, Z. Wu, Y. Jiang, W. Liu, X. Li, B. Jiao, W. Abbas, X. Hou, A flexible and thin graphene/silver nanowires/polymer hybrid transparent electrode for optoelectronic devices, ACS Appl. Mater. Interfaces 8 (45) (2016) 31212–31221.
[158] H. Lu, J. Sun, H. Zhang, S. Lu, W.C. Choy, Room-temperature solution-processed and metal oxide-free nano-composite for the flexible transparent bottom electrode of perovskite solar cells, Nanoscale 8 (11) (2016) 5946–5953.

[159] K.K. Sears, M. Fievez, M. Gao, H.C. Weerasinghe, C.D. Easton, D. Vak, ITO-Free flexible perovskite solar cells based on roll-to-roll, slot-die coated silver nanowire electrodes, Solar RRL 1 (8) (2017) 1–9.
[160] P. You, Z. Liu, Q. Tai, S. Liu, F. Yan, Efficient semitransparent perovskite solar cells with graphene electrodes, Adv. Mater. 27 (24) (2015) 3632–3638.
[161] I. Jeon, J. Yoon, N. Ahn, M. Atwa, C. Delacou, A. Anisimov, E.I. Kauppinen, M. Choi, S. Maruyama, Y. Matsuo, Carbon nanotubes versus graphene as flexible transparent electrodes in inverted perovskite solar cells, J. Phys. Chem. Lett. 8 (21) (2017) 5395–5401.
[162] I. Jeon, T. Chiba, C. Delacou, Y. Guo, A. Kaskela, O. Reynaud, E.I. Kauppinen, S. Maruyama, Y. Matsuo, Single-walled carbon nanotube film as electrode in indium-free planar heterojunction perovskite solar cells: investigation of electron-blocking layers and dopants, Nano Lett. 15 (10) (2015) 6665–6671.
[163] H. Sung, N. Ahn, M.S. Jang, J.K. Lee, H. Yoon, N.G. Park, M. Choi, Transparent conductive oxide-free graphene-based perovskite solar cells with over 17% efficiency, Adv. Energy Mater. 6 (3) (2016) 1–6.
[164] D. Lasrado, S. Ahankari, K. Kar, Nanocellulose-based polymer composites for energy applications-A review, J. Appl. Polym. Sci. 137 (27) (2020) 1–14.
[165] A.T. Vicente, A. Araújo, M.J. Mendes, D. Nunes, M.J. Oliveira, O. Sanchez-Sobrado, M.P. Ferreira, H. Águas, E. Fortunato, R. Martins, Multifunctional cellulose-paper for light harvesting and smart sensing applications, J. Mater. Chem. C 6 (13) (2018) 3143–3181.
[166] L. Gao, L. Chao, M. Hou, J. Liang, Y. Chen, H.-D. Yu, W. Huang, Flexible, transparent nanocellulose paper-based perovskite solar cells, npj Flex. Electron. 3 (1) (2019) 1–8.
[167] H.H. Hsu, W. Zhong, Nanocellulose-based conductive membranes for free-standing supercapacitors: a review, Membranes 9 (6) (2019) 1–21.
[168] I.A. Berhe, W.N. Su, C.H. Chen, C.J. Pan, J.H. Cheng, H.M. Chen, M.C. Tsai, L.Y. Chen, A.A. Dubale, B.J. Hwang, Organometal halide perovskite solar cells: degradation and stability, Energy Environ. Sci. 9 (2) (2016) 323–356.
[169] I. Lee, Y. Jo, D.S. Kim, H.Y. Jeong, Y. Jun, Efficient, durable and flexible perovskite photovoltaic devices with Ag-embedded ITO as the top electrode on a metal substrate, J. Mater. Chem. A 3 (28) (2015) 14592–14597.
[170] Q.F. Lin, L.F. Lu, M.M. Tavakoli, C. Zhang, G.C. Lui, Z. Chen, X.Y. Chen, L. Tang, D.Q. Zhang, Y.J. Lin, P.C. Chang, D.D. Li, Z.Y. Fan, High performance thin film solar cells on plastic substrates with nanostructure-enhanced flexibility, Nano Energy 22 (2016) 539–547.
[171] S. Savagatrup, A.D. Printz, T.F. O'Connor, A.V. Zaretski, D. Rodriquez, E.J. Sawyer, K.M. Rajan, R.I. Acosta, S.E. Root, D.J. Lipomi, Mechanical degradation and stability of organic solar cells: molecular and microstructural determinants, Energy Environ. Sci. 8 (1) (2015) 55–80.
[172] I. Ham, W.J. Dong, J.Y. Park, C.J. Yoo, I. Lee, J.L. Lee, A challenge beyond bottom cells: top-illuminated flexible organic solar cells with nano-structured dielectric/metal/polymer (DMP) films, Adv. Mater. 27 (27) (2015) 4027–4033.
[173] I. Wang, W.L. Feng, J. Du, W.N. Xue, L.L. Zhang, L.L. Zhao, Y. Li, X.H. Zhong, Cosensitized quantum dot solar cells with conversion efficiency over 12%, Adv. Mater. 30 (11) (2018).
[174] I. Li, H.Y. Zhen, L.Y. Niu, X. Fang, Y.K. Zhang, R.S. Guo, Y. Yu, F. Yan, H.F. Li, Z.J. Zheng, Full-solution processed flexible organic solar cells using low-cost printable copper electrodes, Adv. Mater. 26 (42) (2014) 7271–7278.
[175] I.L. Zhang, K. Aitola, C. Hagglund, A. Kaskela, M.B. Johansson, K. Sveinbjornsson, E.I. Kauppinen, E.M.J. Johansson, Dry-deposited transparent carbon nanotube film as front electrode in colloidal quantum dot solar cells, ChemSusChem 10 (2) (2017) 434–441.
[176] G.I. Koleilat, I.J. Kramer, C.T.O. Wong, S.M. Thon, A.J. Labelle, S. Hoogland, E.H. Sargent, Folded-light-path colloidal quantum dot solar cells, Sci. Rep. 3 (2166) (2013) 1–5.
[177] C.H.M. Chuang, P.R. Brown, V. Bulovic, M.G. Bawendi, Improved performance and stability in quantum dot solar cells through band alignment engineering, Nat. Mater. 13 (8) (2014) 796–801.
[178] I.N. Gao, E. Talgorn, M. Aerts, M.T. Trinh, J.M. Schins, A.J. Houtepen, L.D.A. Siebbeles, Enhanced hot-carrier cooling and ultrafast spectral diffusion in strongly coupled pbse quantum-dot solids, Nano Lett. 11 (12) (2011) 5471–5476.
[179] A.E. Semonin, J.M. Luther, S. Choi, H.Y. Chen, J.B. Gao, A.J. Nozik, M.C. Beard, Peak external photocurrent quantum efficiency exceeding 100% via MEG in a quantum dot solar cell, Science 334 (6062) (2011) 1530–1533.
[180] I. Kumar, S. Kannappan, S. Ochiai, P.K. Shin, High-performance organic solar cells based on a low-bandgap poly-thienothiophene-benzodithiophene polymer and fullerene composite prepared by using the airbrush spray-coating technique, J. Korean Phys. Soc. 62 (8) (2013) 1169–1175.
[181] V.A. Akhavan, B.W. Goodfellow, M.G. Panthani, D.K. Reid, D.J. Hellebusch, T. Adachi, B.A. Korgel, Spray-deposited $CuInSe_2$ nanocrystal photovoltaics, Energy Environ. Sci. 3 (10) (2010) 1600–1606.
[182] I.J. Kramer, G. Moreno-Bautista, J.C. Minor, D. Kopilovic, E.H. Sargent, Colloidal quantum dot solar cells on curved and flexible substrates, Appl. Phys. Lett. 105 (16) (2014).
[183] I.T. Li, L. Wei, C.C. Wu, C. Liu, Y.X. Chen, H. Liu, J. Jiao, L.M. Mei, Flexible quantum dot-sensitized solar cells with improved efficiencies based on woven titanium wires, J. Mater. Chem. A 2 (37) (2014) 15546–15552.
[184] I. Cho, P. Giraud, B. Hou, Y.W. Lee, J. Hong, S. Lee, S. Pak, J. Lee, J.E. Jang, S.M. Morris, J.I. Sohn, S. Cha, J.M. Kim, Charge transport modulation of a flexible quantum dot solar cell using a piezoelectric effect, Adv. Energy Mater. 8 (3) (2018).
[185] X.L. Zhang, P.K. Santra, L. Tian, M.B. Johansson, H. Rensmo, E.M.J. Johansson, Highly efficient flexible quantum dot solar cells with improved electron extraction using MgZnO nanocrystals, ACS Nano 11 (8) (2017) 8478–8487.
[186] M. Asaduzzaman, M. Hasan, A.N. Bahar, An investigation into the effects of band gap and doping concentration on Cu (In, Ga) Se 2 solar cell efficiency, SpringerPlus 5 (2016) 1–8.
[187] N. Mufti, T. Amrillah, A. Taufiq, M. Diantoro, H. Nur, Review of CIGS-based solar cells manufacturing by structural engineering, Sol. Energy 207 (2020) 1146–1157.
[188] J. Ramanujam, D.M. Bishop, T.K. Todorov, O. Gunawan, J. Rath, R. Nekovei, E. Artegiani, A. Romeo, Flexible CIGS, CdTe and a-Si: H based thin film solar cells: a review, Prog. Mater. Sci. 110 (2020) 1–20.
[189] B. Stegemann, F. Fink, H. Endert, M. Schüle, C. Schultz, V. Quaschning, J. Niederhofer, H.U. Pahl, Novel concept for laser patterning of thin film solar cells: complete structuring of chalcopyrite solar cells with nanosecond laser pulses, Laser Tech. J. 9 (1) (2012) 25–29.
[190] Y.-C. Wang, T.-T. Wu, Y.-L. Chueh, A critical review on flexible Cu(In, Ga)Se_2 (CIGS) solar cells, Mater. Chem. Phys. 234 (2019) 329–344.